A Model Study on Water Soluble Polymeric Nanofibers for Rapid Flocculation and Enhanced Dewatering of Fine Oil Sands Tailings Simulated Through Kaolin

by

Christopher Afacan

A thesis submitted in partial fulfillment of the requirements for the degree of
Master of Science

in

Chemical Engineering

Department of Chemical and Materials Engineering

University of Alberta

Abstract

Nanofibers are fibers with diameters lower than 100 nm, traditionally made from natural or synthetic polymers. Properties of nanofibers, such as low density, controllable surface functionality, and high surface area to volume ratio, allowed researchers to use them in a multitude of applications such as filtration, cosmetics, and drug delivery. The most common method to produce nanofibers is electrospinning because it is robust and straightforward to setup. However, the relatively low yield and high cost of producing nanofibers by this method has been a major hurdle in its industrial exploitation. In this study, this method was improved upon to increase the output of nanofibers generated by bubble spinning. Instead of a needle producing a single thread of fiber, a continuous process of forming bubbles in a polymer solution was used which created hundreds of threads when the bubbles broke.

Hot water is used to remove bitumen from oil sands ores. The tailings produced from this process contain a mixture of clays, sands, salts, and residual bitumen. These tailings are disposed into open pits called tailing ponds to allow further settlement of solids. However, these tailings ponds are toxic to the environment and require large amounts of land that is difficult to reclaim. The mature fine tailings (MFT) layer in tailings ponds, produced by the bitumen extraction processes, consists of fine particle and water suspensions that take several years to settle. This poses a major environmental problem.

Recently, rapid flocculation and dewatering of oil sands tailings using polymeric nanofibers has been considered. Water-soluble polymers, combined with flocculation techniques, have been used in the industry to efficiently release entrapped water by bridging small particles to create large, heavier flocs, which can then settle. Currently, there is no technology that can effectively dewater MFT to desired levels of solids content because of the high water retention resulting from the use of polymeric flocculants. Due to their immediate initial interaction with fine particles and the nanofiber length, polymer nanofibers have the potential to perform better than their parent polymers. To further understand the mechanism and the effect of these nanofibers on mature fine tailings compared to their original polymer counterparts, a model study was conducted in a less complicated environment. Kaolin was used throughout this analysis since it is one of the major clay minerals in MFT. Poly(acrylamide-co-diallyldimethylammonium chloride) was chosen as it is commercially available and currently being used in industry. The original polymer was also fabricated as a powder to further reduce variability during flocculation tests. The initial settling rate, turbidity of supernatant, water recovery, capillary suction time, and solid content were measured to determine the effect of nanofibers on the solid-liquid separation. In addition to the kaolin flocculation tests, MFT trials were conducted to further investigate nanofiber performance compared to the equivalent polymer solution and polymer powder.

It was shown that the solid forms of the polymer (either as nanofiber or powder) perform better than the polymer solution throughout each test, with optimum dosages of 5 wt. % MFT loading. Nanofibers were able to achieve settling rates of 60 m/h while the other forms were only able to achieve 42 m/h. Additionally, the turbidity of the supernatant obtained after flocculation with nanofibers was 15 NTU, while the polymer solution and powder produced turbidites of 162 and 70 NTU, respectively. Polymer nanofibers and powder generated larger flocs compared to the polymer solution, which produced small, homogenized flocs. The kaolin studies showed that polymer nanofibers could absorb onto clay particles faster and produce flocs more rapidly due to their high surface area to volume ratio. Our results indicate that polymer nanofibers, as well as polymer powders, may be successfully used to treat the MFT produced from oil sands.

Preface

Chapter 3 of this thesis will be submitted for publication as Afacan, C.; Narain, R.; Soares, J.B.P. "A Model Study on Water Soluble Polymeric Nanofibers for Rapid Flocculation and Enhanced Dewatering of Fine Oil Sands Tailings Simulated Through Kaolin."

Chapter 4 of this thesis will be submitted for publication as Afacan, C.; Narain, R.; Soares, J.B.P. "Water Soluble Polymeric Nanofibers for Rapid Flocculation and Enhanced Dewatering of Mature Fine Tailings."

Acknowledgements

Firstly, I would like to thank my supervisors Dr. Joao B.P. Soares and Dr. Ravin Narain for their guidance, encouragement, support, and patience, as well as their vast knowledge. Under their supervision, I have gained numerous skills, theoretical knowledge, and practical experience that have allowed me to become an effective independent researcher that I will not take for granted.

I would like the express my deepest gratitude to both Dr. Soares's and Dr. Narain's research groups, past and present. It was a pleasure to know each and every one of them and it was a joy to come into the labs and work with them.

I would like to thank my friends and family, especially my parents and my sister. Nobody has been more important to me in the pursuit of this project than the members of my family. I would like to thank my parents; whose love and guidance are with me in whatever I pursue.

I would also like to thank my girlfriend, Davina, for always pushing me and believing in me. Without her cheerful self in my life, long days of lab work would blend together.

Finally, I would like to thank my brother, Greg. Without him would have made this much harder and as much as this is my research, a part of him will always belong to this work.

Table of Contents

List of Figures

List of Tables

Nomenclature

Al - PAM	Aluminum hydroxide polyacrylamide
CST	Capillary suction time
DADMAC	Poly (diallyl dimethyl ammonium chloride)
D.C	Direct current
FBRM	Focused beam reflectance measurement
FFT	Fluid fine tailings
FTIR	Fourier transform infrared
GPC	Gel permeation chromatography
HPAM	Hydrolyzed polyacrylamide
ISR	Initial settling rate
LCST	Lower critical solution temperature
MFT	Mature fine tailings
PAA	Polyacrylic acid
PAM	Polyacrylamide
P(Am-*co*-DADMAC)	Poly (acrylamide-*co*-diallyldimethylammonium chloride)
PAMN	Poly (2-aminoethyl methacrylamide hydrochloride)-*st*-(N-isopropylacrylamide)
PNIPAM	Poly (N-isopropylacrylamide)
QCM-D	Quartz microbalance with dissipation
SAGD	Steam assisted gravity drainage

Chapter 1 - Introduction

Bitumen is a highly sought after commodity that can be processed, or upgraded, to produce asphalt concrete, synthetic crude oil, and other petrochemical products. Though the ability to produce these products has vastly improved quality of life, they have also had a substantial negative effect on the environment. Tailings ponds, a by-product of the bitumen extraction process, are filled with toxic waste, and cover (as of 2013) 220 km^2 of Canadian land alone [1]. Tailings ponds generated by mining oil sands ores have potential impacts to the environment such as solid waste, land use and reclamation, in addition to water and air pollution. The largest challenge facing the industry is the reclamation of land occupied by tailings ponds through rapid dewatering of oil sands tailings with new or improved tailings treatment technologies.

1.1 Oil Sands and Oil sands Tailings

1.1.1 Oil Sands Industry in Alberta

Even though Canada has the third largest oil reserves in the world, most, if not all, oil sands operations occur with Alberta [2]. The three major oil sands deposits in northern Alberta are Peace River, Athabasca, and Cold Lake, as seen in Figure 1.1. As of 2014, these oil reserves produce 2.15 million barrels/day of bitumen and is estimated to increase to 3.95 million barrels/day by 2030 [2,3].

Figure 1.1. Alberta oils sands reserves. Figure adapted from [4].

1.1.2 Oil Sands Operations

Figure 1.2 shows the process of extracting bitumen using the Clark hot water extraction process. Bitumen extraction can be done by one of two ways: in-situ production or open pit mining, or a combination of both [5]. In-situ production utilizes steam assisted gravity drainage (SAGD) to recover bitumen that is too deep (>75 meters underground) and too viscous for conventional extraction methods [5,6]. Steam is injected into a well, which lowers the viscosity of bitumen, allowing it to flow and be pumped to the surface.

Open pit mining is the most widely used technique to extract bitumen [7]. This process is similar to mineral mining operations, using large shovels to scoop chunks of oil sands into transportation trucks that are subsequently moved to crushers. Hot water is then added to form a slurry, so it can be pumped to the extraction plant. Bitumen is separated from the coarse solids and recovered using froth treatment. The separation process requires 2.5 m^3 of water for every barrel of bitumen extracted [8,9]. This extraction process produces large volumes of high-water content tailings composed of sand, silt, clay, and residual bitumen. The slurry of water, bitumen, and fines are discharged into tailings ponds as fluid fine tailings (FFT) for solid-liquid separation [10].

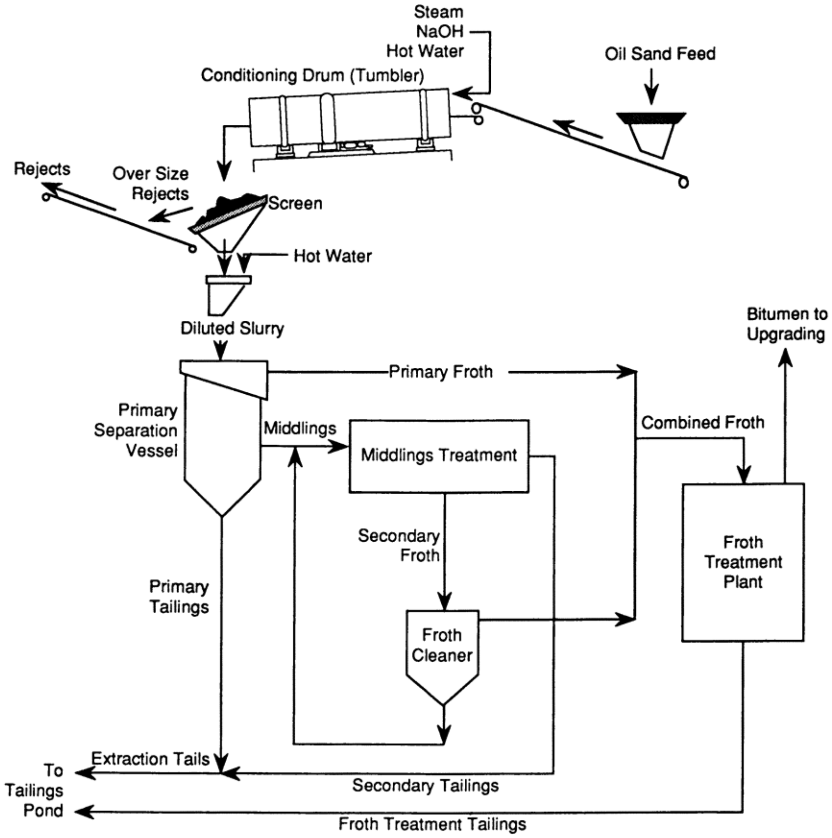

Figure 1.2. Schematic of traditional bitumen extraction process. Figure adapted from [11].

1.1.3 Oil Sands Tailings

Figure 1.3 shows a cross section of a tailings pond. When the tailings are discharged to the tailings ponds, the tailings separate into three layers. Heavy, coarse sand settles to the bottom fairly quickly, forming a beach. Recyclable water released from the tailings form the top layer. The finer solids form an aqueous suspension of fine particles (fluid fine tailings). Fluid fine tailings (FFT) are composed of approximately 55 wt. % solids, of which 82 wt. % is sand and 17 wt. % are fines smaller than 44 μm, and 1 wt. % bitumen [13]. The majority of the fines is made up of clay minerals such as kaolin (55%) and illite (20%). Over a period of years, more fines settle out, creating a stable, gel-like suspension known as mature fine tailings (MFT) containing approximately 30 wt. % solids with a high-water retention capacity [14, 15]. This MFT has little to no consolidation rate, creating serious environmental and economic problems. Oil production creates more and more tailings, thus increasing the amount of land required for their storage. If current tailings management practices do not improve, it is estimated that the amount of MFT will grow to 2 billion m^3 by 2034 [16]. A large amount of research into accelerating the settling rates of the fine particles in MFT and enhancing the water recovery trapped in the tailings has been carried out. Dewatering technologies include physical/mechanical, natural, and chemical processes.

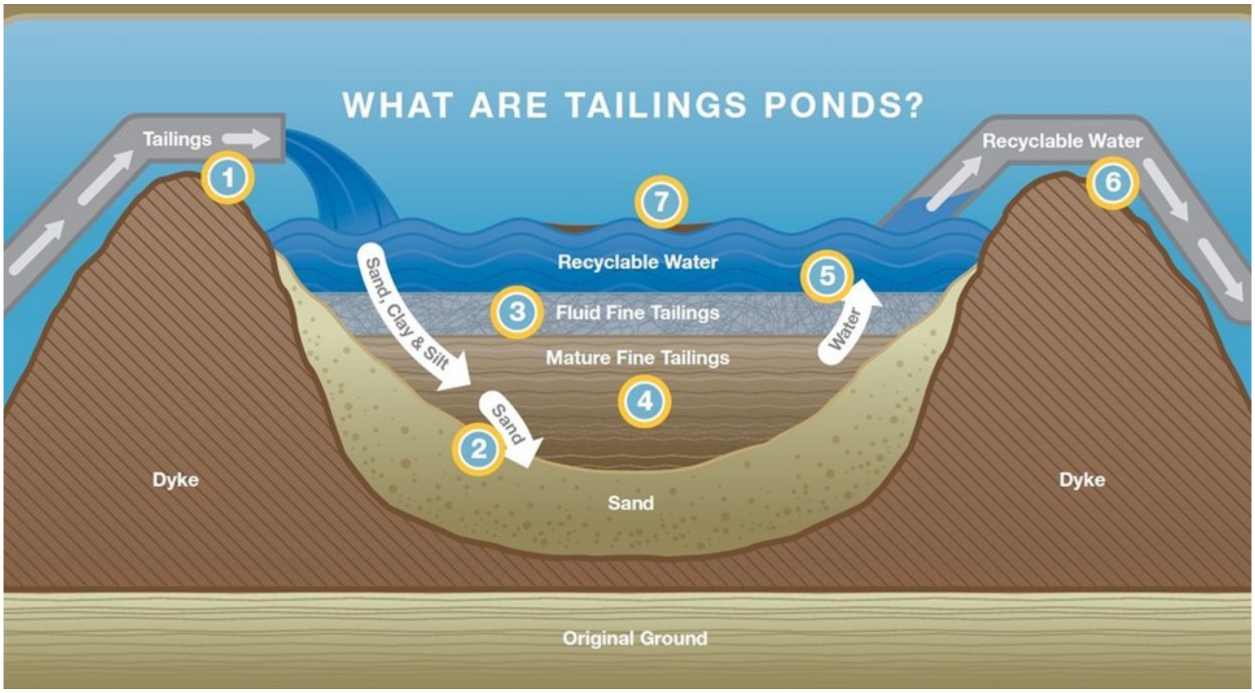

Figure 1.3. Cross section of a tailings pond. Figure adapted from [12].

1.1.4 Technologies for the Treatment of Oil Sands Tailings

Dewatering technologies through physical/mechanical processes include, but are not limited to filtration, centrifugation, and electrical treatment. Filtration is the most common of the physical treatments because of its low environmental impact, but it suffers from capital and operating cost [10]. Additionally, the number of fines play a large role in the efficiency of filtration. Filtering whole tailings with fines greater than 10% becomes problematic without the addition of flocculant [17]. Centrifugation can produce large improvement in solids content and water recovery, increasing the solids in tailings from 30% to approximately 60% [18, 19]. Electrical treatments can also improve settling rates. During electrical treatment, a direct current (DC) electric field is applied to the clay slurry. The negatively charged kaolinite particles will then move toward the positive electrode (anode), increasing the settling rate [20]. Although these methods are effective, they require experienced operators and operation costs are high.

Natural processes involve utilizing environmental or geophysical processes to dewater oil sands tailings. The most traditional technique is freeze-thaw dewatering. Simply, the mature fine tailings are discharged over a large surface and are allowed to freeze during winter. During the following summer, the oil sands thaw allowing the entrained water to be drained and reused in the bitumen extraction process. The increased water release is due to the physical rejection and subsequent aggregation of interstitial minerals and ionic impurities caused by the solidification of pore water [21]. Through freeze – thaw, the solids content of MFT can increase from 30% to approximately 45% [22].

Chemical treatments use densification technologies such as coagulants (consolidated tailings) or flocculants (paste technology) to change the properties of MFT to remove water. Coagulants such as gypsum or alum can be added to MFT to neutralize negatively-charged particles and reduce repulsion, causing them to coagulate in flocs. Flocs are then able to settle through gravity, as flocs size increases due to more collisions between the flocs. The problem with this technique is the high concentration of bivalent cations introduced in the recovered water which cannot be recycled to the bitumen extraction process without further refining [23]. Additionally, flocs produced by coagulation are delicate and have low shear resistance [24]. This may cause breakage during transportation. Paste technology uses polymer flocculants to settle suspended particles in the MFT and densify its sediments [10,23]. Depending on the polymer's characteristics, destabilization of clay in MFT is caused by charge neutralization, charge patching, and bridging. The major downside to these flocculants is that they can be expensive to synthesize and can retain a large amount of water in the sediments [23, 25]. Recently, water-soluble polymeric nanofibers have been considered as novel flocculants, because they can induce rapid flocculation and dewater mature fine tailings effectively.

1.2 Problem Statement

In July 2016, the Province of Alberta introduced Directive 085 that required oil sands operators to improve and accelerate the methods by which they deal with MFT production, storage and treatment. The directive states that all fluid tailings associated with a project must be reclaimed ten years after the end of the project [26]. However, there is no industry-wide technology available to effectively dewater oil sands tailings within this time span that is economically feasible. This can only be achieved if existing dewatering techniques are improved and/or better technologies are developed. In this study, water-soluble polymers were turned into nanofibers and were tested for flocculation in kaolin suspensions and MFT.

1.3 Objectives

This research tested the following hypothesis: Why is the flocculation efficiency of nanofibers different from that of their parent polymers in solution?

The specific objectives of this work are:

1) Fabricate polymer nanofibers from poly(acrylamide-*co*-diallyldimethylammonium chloride), P(Am-*co*-DADMAC), using an improved version of electrospinning (bubble electrospinning).
2) Produce polymer powder from P(Am-*co*-DADMAC).
3) Flocculate kaolin suspensions (as model tailings) with P(Am-*co*-DADMAC) solution, nanofiber, and powder.
4) Flocculate MFT with P(Am-*co*-DADMAC) solution, nanofiber, and powder.
5) Compare the flocculation performances of the three forms of P(Am-*co*-DADMAC).
6) Investigate the mechanisms causing the three forms to behave differently from one another.

Chapter 2 - Literature Review and Theory

2.1 Flocculation

Flocculation is the highly complex process of gathering stable colloids to form large agglomerates (flocs) with the addition of flocculants and/or coagulants. Effective flocculation requires a good understanding of the interaction between fine particles in suspension. Colloidal particles have different sizes, surface charges, and surface functional groups. The stability of fines in suspension is classically described by the DLVO (named after Derjaguin, Landau, Verwey and Overbreek) theory [27]. An electrostatic repulsion force, rereferred to as electrical double layer repulsion, between neighboring particles is produced by the electrical charge on each particle. This electrical repulsion of the surface charges prevents the attraction of particles in colloids due to Van der Waals forces, resulting in the stabilization of the suspension. Therefore, both the type of polymer and how it is applied to a system play a large role in flocculation effectiveness. Destabilization of the suspended particles, floc formation/growth, and floc degradation are the three principle steps in flocculation [28]. Figure 2.1 shows the main flocculation mechanisms of polymers. Depending on their characteristics, polymer flocculants can destabilize and grow clay flocs in MFT using mechanisms such as charge neutralization and bridging, respectively. Generally, flocculants are long-chained polymers that are able to adhere to and interact with a particle surface.

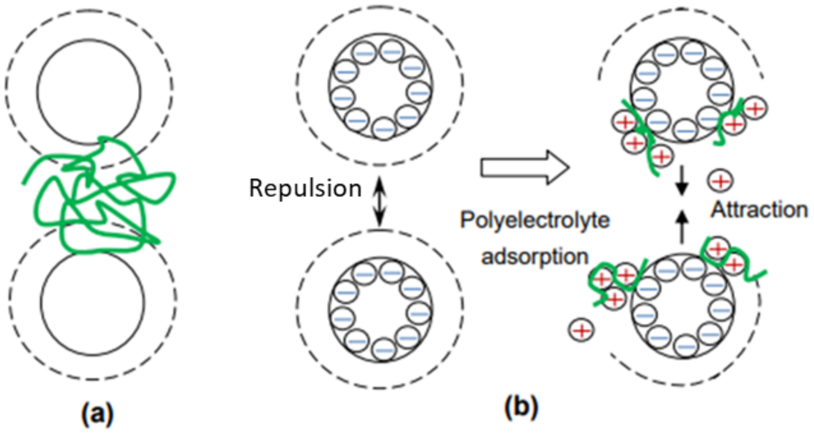

The dashed line represents the range of electric double layer.

Figure 2.1. Illustration of flocculation mechanisms: (a) bridging; and (b) charge neutralization. Figure adapted from [29].

2.1.1 Types of Flocculants

There are two types of flocculants: inorganic and polymeric. Inorganic flocculants such as alum and gypsum are salt based, and are generally referred to as coagulants. They are cheap, easy to use, and reliable. Coagulants hydrolyze in water producing anions and cations which neutralize charged suspended particles, causing them to coagulate in flocs [30]. Increase in floc size is due to an increase in the collision rate caused by Brownian motion.

Polymeric flocculants can be further categorized as synthetic or natural. Natural polymers such starch, chitosan, cellulose, alginate, and guar guam are used because they are bio-degradable, non-toxic, renewable, and easily available [31, 32]. However, they suffer from poor flocculation performance (compared to synthetic polymers) and have short storage life. Synthetic polymers are the most common flocculants because of their ability to be tailored to specific applications [7, 32]. Commercial flocculants are generally water soluble and commonly based on acrylamide and acrylic monomers. Frequently used synthetic polymers for MFT treatment include polyacrylamide (PAM), polyacrylic acid (PAA), and poly(diallyl dimethyl ammonium chloride) (DADMAC) [33]. These polymers are inexpensive and easy to produce. However, most polymer flocculants are hydrophilic, causing them to retain a significant amount of water inside floc pores and have to be used in conjunction with mechanical dewatering techniques to further improve water recovery.

2.1.2 Parameters that Effect Flocculation

Polymer and tailings properties, as well as operational parameters used during the flocculation process, can positively or negatively affect solid-liquid separation efficiency. This includes polymer molecular weight and dosage, solution pH, particle size, and mixing conditions.

The molecular weight of a polymer plays a large role in its flocculation efficiency. It is generally accepted that the larger the molecular weight of the polymer, the better it is at separating solids and liquid. Flocculants with high molecular weights have longer chains compared to low molecular weight polymers, and thus are better able to bridge particles together by absorbing on multiple particles at the same time. Therefore, high molecular flocculants can settle fines faster than low molecular weight polymers [34].

Additionally, polymer dosage can have a significant effect on flocculation efficiency. As polymer dosage increases, flocculation efficiency increases. There is an optimal dosage at which polymers achieve the best settling rate. The amount of polymer that is deemed optimal occurs when there is partial coverage of the particle surfaces, approximately half of the area, which still allows the remaining available surface space to interact with other polymer chains, facilitating polymer bridging of two or more particles [35, 36]. When polymer dosage is below the optimum, polymer bridging is insufficient, leading to unlinked particles in the supernatant of the suspension. When polymer dosage is higher than the optimum, the flocculation performance decreases due to steric stabilization: the particle surfaces become fully covered with polymer, hindering further polymer adsorption and bridge formation.

Altering the pH of the solution can change the surface charge of the mineral particles in suspension, as well as the shape and structure of the polymers. At lower pH values, fine clays have lower charges, allowing for easier flocculation. At higher pH values, clays become more negatively charged. As a result, flocculation becomes more difficult because of the increased repulsion between particles [37].

Increased repulsion can also be caused by an increase in particle surface area per unit volume (decreasing particle size of solids). This increase in particle surface area increases the charge density on the particles, increasing the repulsion and distance between particles [34]. This also increases the time required to sediment smaller particles.

Mixing conditions can also influence the performance of a given flocculant. Mixing (shear) is used to increase collisions between flocculant macromolecules and particles in suspension [38]. This will lead to greater polymer adsorption and the generation of flocs. To maximize the effectiveness of the flocculant, optimization of variables such as duration, intensity of agitation, and the equipment used is required. Excellent flocculants can show average performance if optimal operating conditions are not used [39]. Excessive mixing time or agitation can break the flocs, which is detrimental because further polymer adsorption will occur on smaller flocs, subsequently exceeding the optimum polymer dosage [7,40].

2.1.3 Previous Studies of Tailings Treatment using Flocculates

Developing new and/or improving current technologies is essential to further recover water used in the extraction process and to reduce the volume of tailings stored in ponds. Most polymer flocculants are based on PAM or hydrolyzed polyacrylamide (HPAM). As previously mentioned, these types of polymers can be tailored to specific applications in different industries by the addition of comonomers (such as DADMAC), partial hydrolysis, or by varying the polymer molecular weight. Although PAM can induce effective solid-liquid separation, its hydrophilic nature causes flocs to retain a significant amount of water, resulting in low-density floccules. Thus, additional dewatering techniques are required. Attempts to improve this have employed copolymers or hybrids of commercial polymers. In addition, temperature-responsive, pH-responsive, and natural polymers have also been studied. Recently, the use of polymeric nanofibers has also been evaluated.

Some researchers have addressed the limitation of hydrophilic polymers by copolymerizing hydrophilic and hydrophobic monomers, allowing sediments to hold less water [41]. Polyethylene can be synthesized with polar functional groups to make both hydrophilic and hydrophobic flocculants. Botha et al. (2017) saw an increase in settling rates, lower capillary suction times (CST) and turbidities, as well as more compact sediments when compared to PAM [42]. However, the synthesis of this polymer is complex, and scale up may prove to be a challenge.

To accelerate settling rates and enhance dewatering, researchers have synthesized inorganic/organic hybrid polymeric flocculants such as aluminum hydroxide-polyacrylamide (Al-PAM), calcium chloride-polyacrylamide, ferric chloride-polyacrylamide, magnesium hydroxide-polyacrylamide, and magnesium chloride-polyacrylamide. Many studies have shown that Al-PAM could outperform commercial PAM flocculants during flocculation tests using kaolinite suspensions. The catatonic nature of the hybrid component ($Al(OH)_3$) promotes charge neutralization, allowing fine solids to come closer to each other while the longer chains of the hybrid macromolecules help bridge particles into larger flocs [43-45].

Stimuli-sensitive polymers have also been considered for improved settling and consolidation performance. Temperature-responsive poly(N-isopropylacrylamide) (PNIPAM) and its derivatives have been used as novel flocculants to treat MFT [46-48]. The water solubility of PNIPAM can be affected by changing the temperature. PNIPAM has a sharp phase transition from a hydrophilic to a hydrophobic state when above its lower critical solution temperature (LCST). Below this temperature PNIPAM can absorb onto particle surfaces via hydrogen bonding, which results in aggregation and rapid settling. By increasing the temperature beyond the LCST, the chains collapse due to the hydrophobic nature of the polymer, further increasing sediment consolidation and dewatering [49]. However, this method may not be economically viable because of the energy cost associated with increasing the temperature of large volumes of MFT above the LCST.

Similar to temperature-responsive polymers, pH-sensitive polymers can further consolidate sediments to increase water recovery. By adjusting the pH during the settling phase, when the polymer is not charged, flocculation and sedimentation occurs. During the consolidation phase, strong adhesion needs to be reduced to dissemble big flocs into small particles. This is done by adjusting the pH, so the polymer can become charged, which creates a repulsion between the particles [50]. Lu et al. (2015) presented a novel flocculant containing a pH-responsive benzobroxole-based polymer, poly[(2-aminoethyl methacrylamide hydrochloride)-*st*-(N-isopropylacrylamide)] (PAMN). By adjusting the pH from 7 to 11, the use of PAMN dramatically increased sediment compatibility and water released compared to NIPAM and NIPAM-based cationic copolymers [51]. Despite its improved water recovery, as with temperature-responsive polymers, synthesis is complex and scale-up may prove to be a significant hurdle.

Natural polymers have the advantage of being nontoxic, renewable, biodegradable, and readily available. They are generally made up of starch, chitosan, and cellulose. To overcome their low water solubility and to increase their flocculation performance, they can be modified with suitable functional groups, as well as by grafting PAM and other water-soluble chains onto them [52,53]. Pennetta de Oliveira et al. (2018) successfully modified chitosan with 3-chloro-2-hydroxypropyltrimethylammonium chloride (Chito-CTA), as well as grafted PAM onto chitosan (Chito-g-PAM), and compared their flocculation efficiency with that of cationic PAM. They concluded that both bio-based polymers performed better than cationic PAM with respect to turbidity, capillary suction time, specific resistance to filtration, and floc size due to the hydrophobic core of chitosan [54].

Recently, cellulose nanofibers have been used in various wastewater treatment applications such as metal adsorption, mineral (quartz and hematite) flotation and flocculation, as well as flocculation of municipal wastewater and kaolin clay suspensions because of their abundance and low environmental impact [55-57]. It has been shown that cellulose nanofibers can effectively flocculate kaolin suspensions, while also providing strong shear resistance of induced flocculation because of their very large specific surface areas and high crystallinity [57-59]. However, despite promising results, cellulose nanofibers have to be used in conjunction with a coagulant or commercial flocculant to reach their full potential and are very sensitive to pH. While kaolin suspensions can provide a simple model to simulate MFT, there has been little to no studies on water-soluble polymeric nanofibers on MFT.

2.2 Nanofibers

Polymers (natural or synthetic) can be made into nanofibers with diameters that are less than 100 nm. Nanofibers have high surface area to volume ratio, small pore size, high pore volume, low density, controllable surface functionality, and high electric and thermal conductivity. The most common method to produce nanofibers is by electrospinning because of its robustness. The concept of electrospinning was first introduced in 1902 by John F. Cooley [60]. His apparatus allowed nitrocellulose solutions to flow through a gas nozzle into an electrical field created by charged electrodes. As a result, a solution jet could be ejected from the polymer solution droplet and subsequently collected onto a drum. Polymer solution droplet deformation in an electric field prior to jetting was further understood by the contribution of Geoffrey Taylor in 1964 [61]. There has been a substantial increase in research concerning nanofiber production and their applications in recent years.

2.2.1 Fabrication

Figure 2.2 shows a traditional electrospinning set up. Three main components are used in this process: a syringe attached with a metal spinneret, a high-voltage power supply, and a grounded collector covered with a conductive sheet of foil. Polymer is dissolved in a solvent and placed inside a syringe. One electrode of the direct current (DC) power supply is connected to the metal spinneret (positive potential) while the other electrode is connected to the collector (negative potential) placed approximately 20 cm away from the needle tip. The solution is then pumped slowly, at a steady rate of 1.5 mL/h, towards the end of the spinneret where is forms a spherical droplet. The droplet is exposed to the electric field and becomes highly electrified, inducing charges that are evenly distributed over the surface. At this point, the droplet experiences three competing forces: an electrostatic repulsion of the surface charges resulting in expansion of the droplet, surface tension of the solution trying to reduce the surface area of the droplet, and resistance to flow due to the viscosity of the polymer solution. As the voltage is increased, the drop is distorted into a conical object known as a Taylor cone [61, 63, 64].

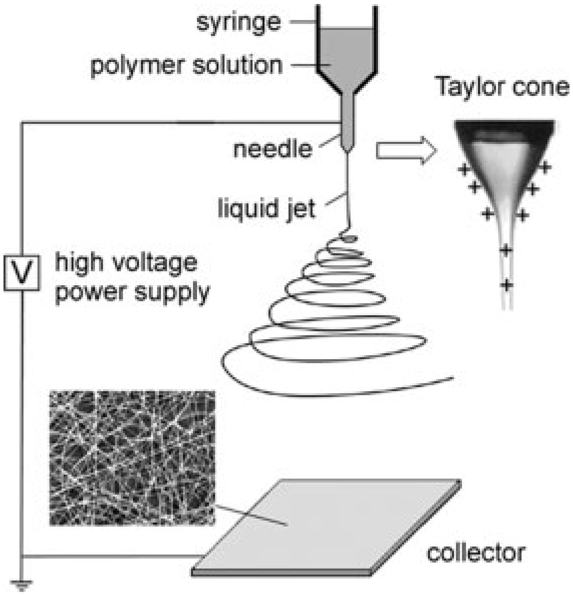

Figure 2.2. Schematic illustration of the basic setup for needle electrospinning. Insets show a Taylor cone as typical SEM of nonwoven nanofibers deposited on the collector. Adapted from [62].

Once the repulsion of surface charges due to the increase in electric field strength surpasses the surface tension and resistance to flow of the solution, a continuous polymer solution jet is ejected from the Taylor cone. This electrified jet experiences a stretching and whipping process due to its unstable nature, which is caused by the continued electrostatic repulsion forces dominating over the surface tension and viscosity of the polymer solution while approaching the collector [65-68]. This causes the jet to undergo elongation due to multiple levels of coiling and recoiling as seen in Figure 2.3. As a result, the jet is deposited randomly onto the collector as dry, thin fibers which can be seen in the SEM image inserted in Figure 2.2.

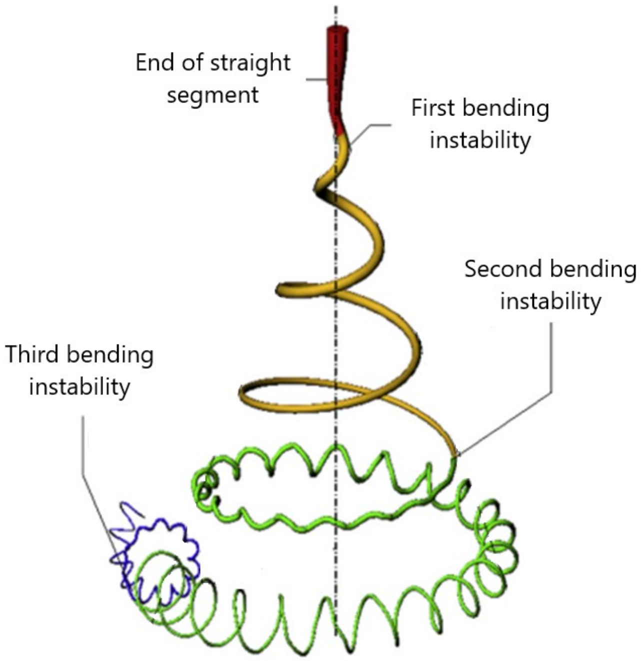

Figure 2.3. Instability of electrified polymer solution jet during electrospinning. Adapted from [69].

2.2.2 Parameters that Affect Fabrication

A multitude of parameters may affect electrospinning. The most common variables include process parameters specific to the electrospinning set up, solution properties, and to a lesser degree, environmental influences while electrospinning [70]. Successful fabrication of nanofibers requires a careful balance of these parameters.

2.2.2.1 Process Parameters

Many variables must be considered when setting up an electrospinning apparatus. These variables include: voltage applied, distance between needle tip and collector, feed rate, as well as the type of collector being used. All of these variables work in conjunction to determine the strength of the electric field acting on the polymer solution jet. Electric field strength is given by equation (2.1),

$$\varepsilon = \frac{V}{d} \tag{2.1}$$

where V is the applied voltage, and d is the distance between the needle top and the collector. Increasing the electric field strength results in thicker fibers due to the increased volume of polymer solution being ejected [71]. If the distance is too small and the voltage is too high, wet fibers will be produced. Thus, voltage and distance must be balanced to ensure ideal nanofiber formation. Feed rate refers to the rate at which the polymer solution is pumped into the spinneret and must be kept constant. Feed rates that are too low will not produce a Taylor cone, while increasing the feed rate can cause an increase in fiber diameter, as well form beads within the fibers [72]. Nanofibers can be aligned or stretched with the help of a rotating drum instead of a stationary collector. If the rotation speed is high enough, the nanofibers can be aligned and stretched, resulting in a reduction of fiber diameter while also eliminating the risk of self-assembly [73-75].

2.2.2.2 Solution Parameters

Different polymers will result in different fiber structures. Solution concentration, viscosity, conductivity, surface tension, as well as the molecular weight of the polymer play an important role in electrospinning efficiency. The most important factor is solution viscosity, which also indirectly affects surface tension. The viscosity of a solution can be changed by increasing the concentration of polymer or by increasing its molecular weight [76]. Generally, there are three phases of production as viscosity increases. At low viscosities, electrospinning is either not possible or beading will occur in the fibers. At the intermediate phase, as viscosity increases, fiber diameter increases due to the jet's inability to elongate [77,78]. At very high viscosities, surface tension becomes too strong and overpowers the electrostatic repulsion in the Taylor cone. Solution viscosity can also be altered by changing the solvent and/or the temperature of the solution [79, 80]. As the temperature of the solution is increased the molecules are able to move more freely, which reduces the surface tension as well as the viscosity of the polymer solution. Conductivity, or the transfer of charge, also plays an important role in electrospinning. Solutions with zero conductivity cannot be electrospun. As the conductivity of a solution increases, thinner, more uniform fibers can be formed due to the repulsion forces becoming more dominate, allowing the instability in the jet during the whipping process to occur sooner [81]. Adding salts or changing the solvent can increase the polymer solution conductivity.

2.2.2.3 Ambient Parameters

Changes in temperature, pressure, and relative humidity can have a significant effect on the efficiency of nanofiber production. As relative humidity increases, there is an increase in the number of pores in the fiber as well as an increase in the size of these pores [82]. Moisture in the atmosphere can conduct charges away from the jet, decreasing the overall charge on the droplet and jet surface, which would require a stronger electric field to compensate. Therefore, ambient temperature should be kept as constant as possible to ensure nanofiber formation is the same each time the experiment is conducted.

2.2.3 Applications

The simplicity of fabrication set-up in conjunction with the diversity of materials suitable for electrospinning make this technique attractive for a number of applications. Recently, there has been an increase in nanofiber use over a broad range of fields due to their extremely high lengths, high surface area to volume ratios, complex pore structures, and high tensile strengths.

Nanofibers have largely been used in filtration applications. Donaldson Company Inc. claims to be the first to successfully use nanofibers for filtration commercially [83]. They produced a multitude of filters for different applications such as their Ultra-Web HD® filter used in on/off-road trucks and equipment which serves as a base filter that can be improved upon to endure harsher, more abrasive chemical and dust exposure. Additionally, a carbon substrate can be incorporated for processes that experience an accumulation of electrostatic charges. Low fiber diameters allow for a much higher filtration performance with similar operational characteristics. Selectivity of a filtration media can be achieved by incorporating active elements (biologically or chemically) on the surface as part of the structure of the nanofiber, allowing for smart filtration. In this case, entrapment of particles is due to chemical/biological reactions rather than physical capture. Other prototype applications of nanofibers include cigarette filters, catalytic cracking, high temperature filtration media, water-in-oil emulsion separation, as well as ion-exchange, hemodialysis, and biocatalytic filtering media [84].

Electrospun nanofibers have also been extensively assessed for biomedical usages because of their interconnected, porous structures and large surface areas, which mimic the natural extra-cellular matrix for tissue engineering [85, 86]. Nanofibers have properties suitable for cell attachment, growth, and proliferation. Drug delivery has also been studied by incorporating antibiotics, anticancer agents, proteins, DNA and RNA into nanofibers [87]. As mentioned above, the high surface area to volume ratio that nanofibers possess can enhance drug loading and mass transfer properties. Nanofibers can also be used as wound dressings to help cellular respiration and prevent bacterial penetration, as well as promote wound healing through the growth of normal skin with the integration of epidermal growth factors [88].

The properties of textiles can be strongly modified with the introduction of nanofibers. Addition of a layer of nanofibers over textiles can provide advantages in protective clothing, masks, and filters against nanoparticle aerosols. A thin coating of nanofibers was able to retain about 80% of 20 nm size particles and over 50% of 200 nm nanoparticle which was further improved to over 99% retention with an increase in fiber diameter [89]. Vitchuli et al. (2010) were also able to achieve filtration efficiencies greater than 99.5% by depositing nylon-6 nanofibers on nylon/cottons woven fabric without sacrificing air permeability or pressure drop. Subsequently, the filtration ability of the fabric was increased by 250% [90]. Additionally, because of the above average water vapour transport properties of nanofibers, layers of electrospun fibers were able to provide "breathable" protective clothing with respect to allowing evaporative cooling to take place while being lightweight and thin [91]. Self-cleaning textile fibers have also been studied by coaxial electrospinning cellulose acetate and dispersions of nanocrystalline TiO_2 [92]. When exposed to halogen irradiation under light typical of an indoor working environment, fabrics were able to self-clean through photodegradation after multiple staining and re-staining of red wine.

Recently, flocculation applications have also been studied. Most of these studies have been restricted to the flocculation of wastewater, quartz/hematite, or kaolin systems via biodegradable polymers like cellulose [55 – 59]. However, these approaches require the addition of additional coagulants or flocculants to reach their full potential. Flocculating tailings in oil sands operations with nanofibers has not been given much attention. Conducting flocculation tests on kaolin and MFT suspensions with more efficient, commercial polymers such as PAM can provide more insight to the flocculation mechanism with respect to nanofibers.

2.3 Bubble Spinning

To improve the yield of electrospinning, bubble electrospinning, or bubble-spinning, was used. Typically, single needle electrospinning produces 0.1 – 1.0 grams of fibers per hour, depending on the input speed of the polymer through the syringe. A single bubble in the bubble-spinning process can produce 7.5 grams of nanofibers per hour [93]. This can be increased further with the addition of more bubbles. The methodology is similar to needle electrospinning, where a strong electric field is applied to a polymer solution. A Taylor cone is produced as charges build up at the polymer surface. As the charge density passes a threshold caused by the viscosity and surface tension of the polymer, a jet is ejected from the Taylor cone. Solvent evaporates as the jet whips rapidly towards the collector, depositing dry fibers.

The difference between these two processes is that the polymer solution, made up of polymer, solvent, and surfactant, is placed in a reservoir where an inert gas is blown into it from below the solution surface, forming a bubble. The bubble wall then replicates the phenomena the solution droplet experiences during needle electrospinning. Surfactant is used to stabilize the bubble by creating surface tension gradients along the bubble wall. This allows fluid to flow from areas of low surface tension to areas of higher surface tension which are the weaker spots along the bubble wall [94,95]. Figure 2.4 shows the deformation of a single polymer bubble under applied voltage. Similar to needle electrospinning, bubbles undergo similar deformations as droplets [96]. However, due to their larger surface area, a larger applied voltage is required to overcome the surface tension of the bubble. Once the applied voltage is large enough, the bubble forms a Taylor cone shape. The net upward force of the bubble represents the applied voltage and is given by,

$$F_{up} = \pi r^2 (P_i - P_o) + Eq \tag{2.2}$$

where, E is the applied voltage, r is the radius of the bubble, q is the total surface charge, and P_i and P_o are the pressure inside and outside the bubble, respectively. The net downward force, represented by the surface tension of the bubble is given by,

$$F_{down} = 2\pi r T \delta \tag{2.3}$$

where, T is the surface tension, and δ is the thickness of the bubble.

The amount of applied voltage needed to exceed the surface tension, thus ejecting a single jet from the Taylor cone, can be determined by equating Equation (2) and (3). Once the electric field exceeds the critical value to overcome surface tension, a jet is ejected and the bubble breaks, resulting in multiple jets being ejected. Another bubble is then produced to start the process over again.

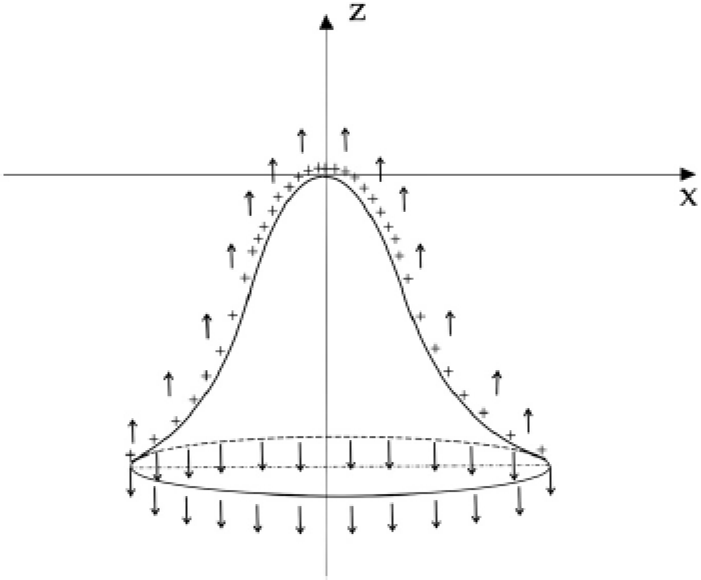

Figure 2.4. Forces action on a polymer bubble under applied voltage. Figure adapted from [97].

If multiple bubbles interact within the system, after the bubble breaks, the ruptured bubble can fold and entrap air as it retracts, subsequently generating smaller “daughter” bubbles which then experience the same process as the parent bubble. Daughter bubbles then break and produce smaller sub-daughter bubbles. [98]. This process occurs within milliseconds and thousands of charged jets are produced.

If there are enough polymer entanglements, the bubble will produce a continuous jet from the apex of the bubble after initial ejection. The bubble then relaxes back to its original hemispherical shape, while jetting continues as the jet carries the charge away. If the electric field strength is increased past this threshold, multiple jets can be formed from the single jet which carry a lower concentration of charge compared to the single jet [99]. Figure 2.5 illustrates a relaxed bubble with a single continuous jet. As electric field strength is increased, more and more jets are produced.

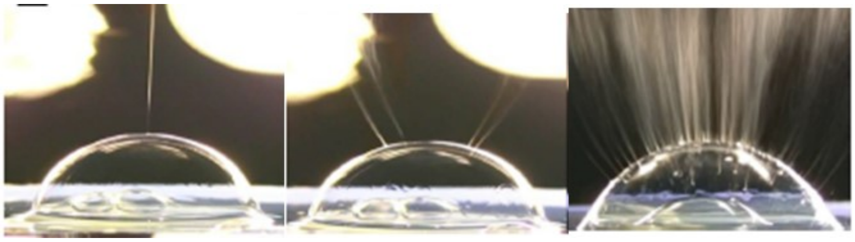

Figure 2.5. Increase in jets on a bubble surface. Figure adapted from [99].

Although there have been more studies on the effects of process, solution, and ambient parameters in traditional electrospinning, parameters affecting bubble-spinning are similar to those in needle electrospinning. Similar to traditional needle spinning, solution concentration and applied voltage can affect fiber diameter. The minimal fiber diameter decreases with increase in applied voltage, while an increase solution viscosity causes an increase in fiber diameter. However, polymer solution viscosity does not influence the quality of nanofibers produced as significantly as for needle electrospinning [100]. Overall, bubble-spinning vastly improves traditional electrospinning techniques is terms of production, simplicity, and robustness.

Chapter 3 - Flocculation and Dewatering of Kaolin

3.1 Introduction

Refined bitumen is a desired commodity and will continue to be for the foreseeable future. However, bitumen extraction is a complicated process that requires many resources, including hot water to extract it from the ground and upgrade it. An unwanted by-product of this process, the production of a slurry waste called tailings, is stored into large areas known as tailings ponds. Tailings are generally made up of solids, bitumen, and water [10]. Tailings ponds are used to separate the coarse solids and release the trapped water by gravity, which can then be recycled to extract more bitumen. The heaviest coarse sands settle to the bottom, while water released from the tailings form the top layer. The middle layer becomes a dense slurry known as mature fine tailings (MFT), which is comprised of approximately 70% water and 30% solids, and experiences practically no further consolidation [101]. Left in this state, MFT could take hundreds of years to achieve minimal consolidation because of the fine clay particles that are held in suspension by electrostatic interactions [102]. The large volume of undesired tailings creates a major environmental problem in terms of contamination of water and soil. As of 2008, more than 750 million m^3 of MFT were stored in tailings ponds in Alberta [10].

A large amount of work has been directed towards accelerating the settling rates of the fine particles in MFT and enhancing the recovery of water trapped in the tailings. Dewatering technologies include natural processes such as evaporation, freeze/thaw, and plant dewatering. Although these processes substantially improve solids content and are inexpensive [10, 21, 22], they are time consuming and labour intensive. Additionally, physical and chemical technologies are being explored. Physical treatments include filtration, centrifugation, thermal drying, and electrical treatment. Filtration is the most common of the physical treatments because of its low environmental impact, but suffers from high handling cost [10, 21, 49]. Centrifugation can produce large improvement in solids content and water recovery, while electrical treatments can improve settling rates; however, operation costs are high, and both require experienced operators. Lastly, in the case of chemical processes, coagulants and paste technology are the most common methods the further consolidate MFT. Coagulants such as gypsum or alum can neutralize negatively charged particles and reduce repulsion between particles. The problem with this technique is the high concentration of bivalent cations introduced in the recovered water which cannot be recycled into the bitumen extraction process without further refining [103]. Paste technology uses polymer flocculates to settle suspended particles in the MFT and densify its sediments [10, 103]. The major downside to these flocculates is that they can be expensive to synthesize. Recently, rapid flocculation and dewatering of mature fine tailings using water soluble polymeric nanofibers has been considered as a potential novel way to treat these tailings.

Nanofibers have diameters lower than 100 nm in diameter, high surface area to volume ratios, small pore sizes, high pore volumes, low densities, controllable surface functionalities, and high electric and thermal conductivities. Nanofibers are traditionally generated by electrospinning (refer to Figure 2.2). During this process, a spinnable solution with optimal viscosity and surface tension is stretched into nanofibers by an electrostatic field (1 – 30 kV) [62, 104]. Since only a single needle and syringe is used to produce the nanofiber, the yield is very low. At a polymer feed rate of 1.5 – 5.0 ml/hr (depending on the polymer), only 0.1 – 1 $g/h/m^2$ of nanofiber can be produced [62, 105]. Bubble electrospinning can increase the output of nanofibers by ten-fold [93]. Instead of a needle producing a single fiber thread, a continuous process forms bubbles in a polymer solution, creating hundreds of fiber threads when the bubble(s) break.

In this study, poly(acrylamide-*co*-diallyldimethylammonium chloride) nanofibers were generated by bubble electrospinning. This polymer was chosen as it is commercially available and already being used in industry to treat tailings. These nanofibers, along with the original polymer solution and polymer powder, were used as flocculants to compare their dewatering efficiency in kaolin suspensions. Kaolin was used as a simple model of MFT because kaolinite makes up 40% to 70% of the solids suspended in MFT [10]. Flocculation studies included the measurement of initial settling rate (ISR), turbidity, water recovery, solids content, sediment dewaterability, floc formation, and floc size. Results show the three forms of poly(acrylamide-co-diallyldimethylammonium chloride) differ in their flocculation/dewatering performance, which indicates that a new form of flocculant for the treatment of mineral tailings may be derived from this innovative concept.

3.2 Materials and Methods

3.2.1 Materials

Poly(acrylamide-*co*-diallyldimethylammonium chloride) solution P(Am-*co*-DADMAC) and surfactant Triton X-100 were purchased from Sigma-Aldrich Chemicals (Oakville, ON, Canada). Kaolin was purchased from Acros Organics. The D10, D50, and D90 of the kaolin particles were 1.94, 6.67, and 27.2 μm, respectively.

3.2.2 Polymer Powder and Nanofiber Fabrication

Figure 3.1 shows the equipment used to produce the nanofibers. A polymer solution was placed in a glass container reservoir with the top open. The glass container was lined with aluminum foil to create more surface area to contact the polymer solution. The positive electrode of a high voltage direct current (D.C) power supply was connected to the lined aluminum foil while the negative electrode was connected to a grounded flat aluminum collector plate placed 10 cm above the reservoir to collect the displaced nanofiber. Multiple bubbles were produced on the free surface of the polymer solution when an inert gas, Nitrogen, was supplied to the bottom of the container. The gas flow rate was controlled with a flow meter to optimize bubble growth. A voltage of 20 kV was applied to the system. When the applied voltage exceeded the threshold voltage, multiple jets were ejected from the bubble. The commercial polymer solution was diluted from 10 wt. % to a predetermined dilution ratio to produce 50 mL of aqueous polymer stock solution with deionized water. For this study, the commercial polymer was diluted from 10 wt. % to 8 wt. %. The stock solution was stirred overnight to enable complete dissolution and obtain optimal solution viscosity for bubble electrospinning. Triton X-100 was added (250 μL) to reduce the surface tension of the polymer solution for easier bubble breaking. The mixture was stirred with the aid of a magnetic mixer at room temperature for 24 hours to ensure complete homogenization. The electrospinning process was then conducted under room temperature.

To obtain P(Am-*co*-DADMAC) in a solid state, the purchased solution was freeze-dried for 1-2 days. The recovered solid polymer was then ground down to a fine powder with a mortar and pestle. This powder form provides an additional control when comparing the performance of nanofibers against its original solution counterpart.

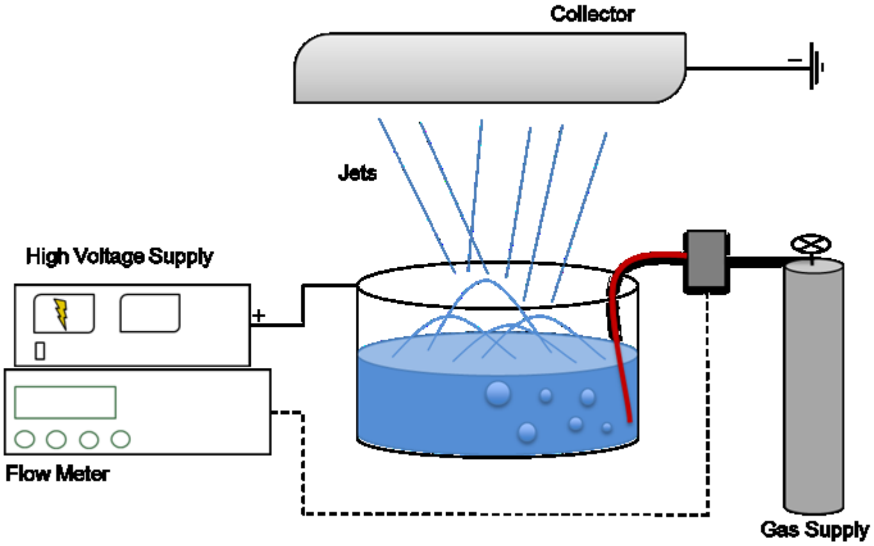

Figure 3.1. Schematic drawing of bubble electrospinning process.

3.2.3 Polymer Characterization

To make sure there was no change in polymer composition during bubble electrospinning, the Fourier transform infrared (FTIR) spectra of the nanofibers were taken using an Aligent Technologies Cary 600 Series FTIR spectrometer. FTIR measurements were carried out in ATR mode. The spectra of nanofiber, solution and powdered polymers were scanned between 400 and 4000 cm^{-1}.

Additionally, polymer molecular weight averages and distributions were measured for polymer solution, powder, and nanofiber by gel permeation chromatography (GPC) (1260 Infinity Multi-Detector GPC/SEC System, Agilent Technologies). For better resolution, two columns (TKS gel G6000PW XL-CP, designed for cationic polymers) were connected in series. Water containing 0.2 M sodium nitrate was used as a mobile phase for the analyses. Polyethylene oxide standards, provided by Agilent Technologies, were used to calibrate the system.

3.2.4 Settling Tests

Dewatering tests included initial settling rate, turbidity of supernatant, water recovery, solids content, and capillary suction time (CST). Nanofiber and polymer dosages ranged from 250 to 1000 ppm (on a mass basis of polymer to solids in suspension). To begin each set of tests, 300 mL of clay solution of 5 wt. % or 10 wt. % solids was prepared by mixing kaolinite clay in deionized water for approximately 30 minutes at approximately 500 rpm. Settling tests were conducted in 100 mL graduated cylinders. Two different procedures were followed, depending on whether polymer nanofiber/powder or solution were being added to the kaolin solution. In the case of nanofiber or powder, the desired dosage of nanofiber/powder was placed in an empty graduated cylinder. Kaolin solution was then added to the cylinder until the level reached 100 mL. In the case of aqueous polymer solutions, 90 mL of kaolin solution was stirred for 2 minutes at 300 rpm to ensure complete homogenization before 10 mL of the aqueous polymer stock solution was added dropwise at a rate of approximately 0.1 mL/s. Stirring was stopped after all polymer was added to the suspension. The mixture was then transferred to 100 mL graduated cylinder. In both cases, the cylinder was inverted 5 times, then left to stand still at room temperature. The height of the mudline (interface of supernatant and sediments) was recorded as a function of time. The sediment was left to settle for 24 hours.

The initial settling rate (ISR) was determined as the initial slope of mudline height versus time curve. Turbidity (NTU) was calculated with the equation [106],

$$NTU \approx 0.191 + 926.1942 \times [-\log\left(\frac{\%T}{100}\right)] \tag{3.1}$$

where $\%T$ is the transmittance of the supernatant measured by a UV-vis spectrometer at 500 nm wavelength. After total removal of the supernatant, the mass of sediments was filtered and dried at 70 ºC for 24 hours. The solids content was calculated by dividing the mass of solid clays after filtration and drying by the total mass of the sediments. Water recovery was determined by dividing the volume of water released by the total volume of kaolin suspension. Capillary suction time was measured using a Triton Electronics meter (Type 319 multi-CST) equipped with Triton filter paper (7 cm x 9 cm) fitted between two Perspex plates with electrode sensors across the top plate. An aliquot (7 ml) of the kaolin suspension was taken and transferred into a cylindrical steel funnel resting on the filter paper. The unit recorded the time taken for the sample to release water through the designated points on the filter paper.

3.2.5 Focused Beam Reflectance Measurement

The change in chord length distribution of flocs before and after the addition of polymer to 5 wt. % kaolin solution was measured using a focused beam reflectance measurement (FBRM) instrument (FBRM G400, Mettler-Toledo, USA). The FBRM probe was used to monitor the particle counts and size distribution in real time during the flocculation process. The probe contains a fast, rotating laser beam that is placed in a 500 mL beaker containing the kaolin slurry. The incident laser beam is reflected from the clay particles and is captured by the FBRM probe. The chord length is calculated by multiplying the beam reflectance speed and the duration of the reflected signal. During the isothermal run, data was collected using a 90 log-channel over the size range of 1–1000 μm. The chord length distribution of flocs was recorded at every 2 seconds during the run. These experiments were carried out with 500 ppm of polymer solution and polymer nanofiber.

3.2.6 Quartz Crystal Microbalance

The interactions between polymer solution, nanofiber, and powder with a silica surface were studied using an E4 QCM-D unit (Q-Sense AB, Gothenburg, Sweden) with silica-coated sensor chips (QSX-303, 5 MHz, AT-cut, Q-Sense AB). All QCM-D experiments were performed in duplicate under flow-through conditions using a digital peristaltic pump at a fixed flow rate of 200 µL/min. The temperature was maintained at 20 ± 0.2 ˚C during experiments. Prior to the experiment, the system was stabilized by injecting ultrapure water for 10 min followed by the injection of 1 mM of a salt solution (pH=8.0) for another 10 min until stable baselines were obtained. The predetermined dosage of polymer was then injected into the QCM chamber for 30 min. Frequency, Δf, and dissipation shifts, ΔD, at 1st, 3rd, 5th, 7th, 9th, and 11th overtones (corresponding to 5, 15, 25, 35, 45, and 55 MHz) were monitored simultaneously. Subsequently, the sensor was washed with the same salt solution followed by ultrapure water. The QCM-D simultaneously measured changes in frequency and dissipation, which could then be used to calculate bandwidths. The small loading approximation can then be followed, which states that the shift of the complex resonance frequency of the QCM is proportional to the ratio of the area-averaged tangential stress and velocity at the crystal surface [107]. The relationship is given as,

$$\frac{\Delta f^*}{N_p} = \frac{\Delta f + i\Delta\Gamma}{N_p} = \frac{f_f}{\pi Z_q} f_{osc} \frac{m\omega(k + i\omega\xi)}{m\omega^2 - (k + i\omega\xi)} \tag{3.2}$$

where f_f is the fundamental frequency (5 MHz), Z_q is the acoustic impedance of AT-cut quartz crystal (8.8×10^6 kg/m^2/s), k is the spring constant, N_p is the number of adhering particles per unit area, ξ is the drag coefficient of the dashpot which quantifies dissipation energy, $\Delta\Gamma$ is the bandwidth, and f_{osc} is the oscillator strength ($0 < f_{\mathrm{osc}} < 1$). In the simplest cases, if a material interacts with the sensor surface strongly ($k >> m\omega^2$), they can move together with the resonator and are termed as inertial loading in the Sauerbrey sense given by [107],

$$\Delta m = \frac{-C\Delta f_n}{n} \tag{3.3}$$

where C is the mass sensitivity constant for a 5 MHz AT-cut quartz crystal (17.7 ng/cm^2 Hz), n is the overtone number (1, 3, 5, 7, 11), and Δf_n is the frequency shift measured at its respective overtone number. Diving by the density of the depositing material yields layer thickness. However, for wake elastic bonding ($k << m\omega^2$), the frequency shift is positive which results in elastic loading.

3.3 Results and Discussion

3.3.1 Nanofiber Production

Table 3.1 compares the number average molecular weight, M_n, weight average molecular weight, M_w, the z-average molecular weight, M_z, and the polydispersity index, PDI, of P(Am-*co*-DADMAC) solution, fiber, and nanofiber. No statistically significant differences are observed among these different forms of P(Am-*co*-DADMAC). Consequently, one may conclude that electrospinning did not causing any chain degradation or cross-linking which could affect the efficiency of the polymer during the flocculation tests [108].

Table 3.1 Molecular weight analysis of P(Am-co-DADMAC) solution, fiber, and nanofiber

Sample	M_n (kDa)	M_w (kDa)	M_z (kDa)	PDI
Solution	320 000	2 400 000	3 900 000	7.6
Powder	370 000	2 900 000	4 700 000	7.8
Nanofiber	340 000	2 700 000	4 600 000	7.8

The FTIR spectra of the original polymer, as well as its nanofiber counterpart, are compared in Figure 3.2. The spectrum for both the nanofiber and polymer solution show similar characteristic frequencies with minor intensity variations summarized in Table 3.2. Among other similarities, both the polymer solution and the nanofiber exhibit pronounced NH_2 stretching vibrations and carboxyl stretching at 3171 cm^{-1} and 1652 cm^{-1}, respectively. Therefore, it can be concluded that there is no change in polymer composition or functionality when the polymer underwent the electrospinning process. The polymer powder was not analyzed by FTIR since it is the same material present in the polymer solution and did not undergo any aggressive treatment that might have altered its chemical composition.

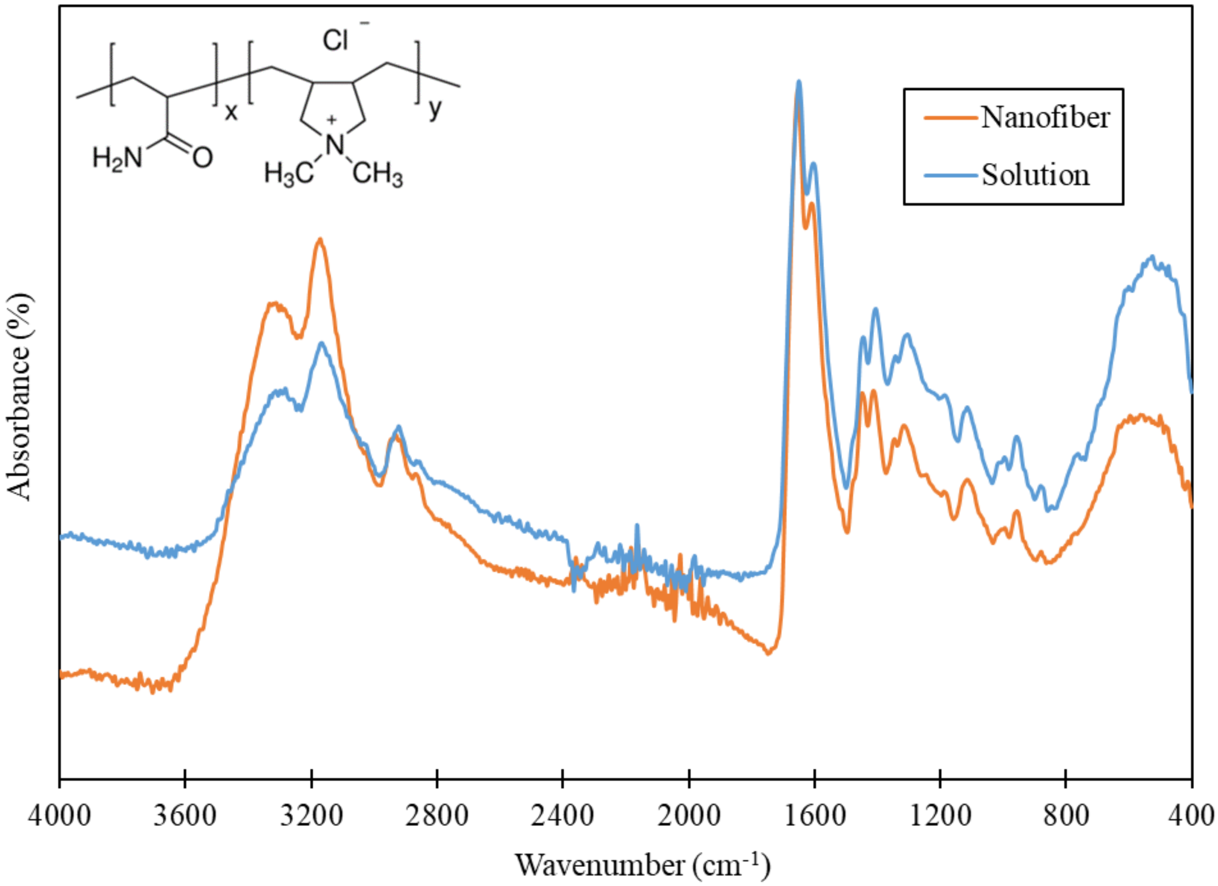

Figure 3.2. FTIR spectra of P(Am-*co*-DADMAC) solution and nanofiber.

Table 3.2 Summary of characteristic wavelengths and their respective assignments.

Wavenumber (cm^{-1})	Assignment
3171	NH_2 stretching vibrations[109 - 112]
2932	-CH_2- stretching[113 – 115]
1652	Carboxyl stretching (C=O)[116, 117]
1608	NH bending vibration[116, 117]
1447	N^+ bonding to dual methylenes[113, 114, 118]
1113	Stretching of C-N bound of heterocycle[113, 114]
955	Quaternary amino[113, 118]

3.3.2 Initial Settling Rate (ISR)

Initial settling rates for 5 wt. % and 10 wt. % kaolin suspensions are shown in Figures 3.3a and 3.3b, respectively. Flocculation experiments were carried out with dosages varying from 250 to 1000 ppm. The control experiment represents the settling of kaolin without addition of any polymer. As expected, all three forms of P(Am-*co*-DADMAC) performed much better than the control across all dosages for both 5 wt. % and 10 wt. % kaolin loading. Polymer-assisted flocculation (in any form) involves neutralizing the negative charges on the clay surfaces with the cationic charges found in DADMAC, and then bridging the clay particles as the non-adsorbed segments (loops and tails) attach to the bare surfaces of other colliding clay particles.

For both solids loading cases, Figure 3.3 shows that the ISR of the kaolin suspensions treated with the polymer solution does not depend on polymer dosage, while the ISR increases with increasing nanofiber dosage. Figure 3.3 also shows that nanofiber and powder forms behave differently. For both kaolin loadings, the nanofiber and powder behave similarly at lower dosages, while the nanofiber performs better at higher dosages.

Among all three forms of P(Am-*co*-DADMAC) delivery, the solution seems to be the most effective, as it reaches higher ISR, meaning that the solids settle at a faster rate than when polymer powder or nanofibers are used, although the differences between polymer solution and nanofibers are not statistically significant at higher dosages.

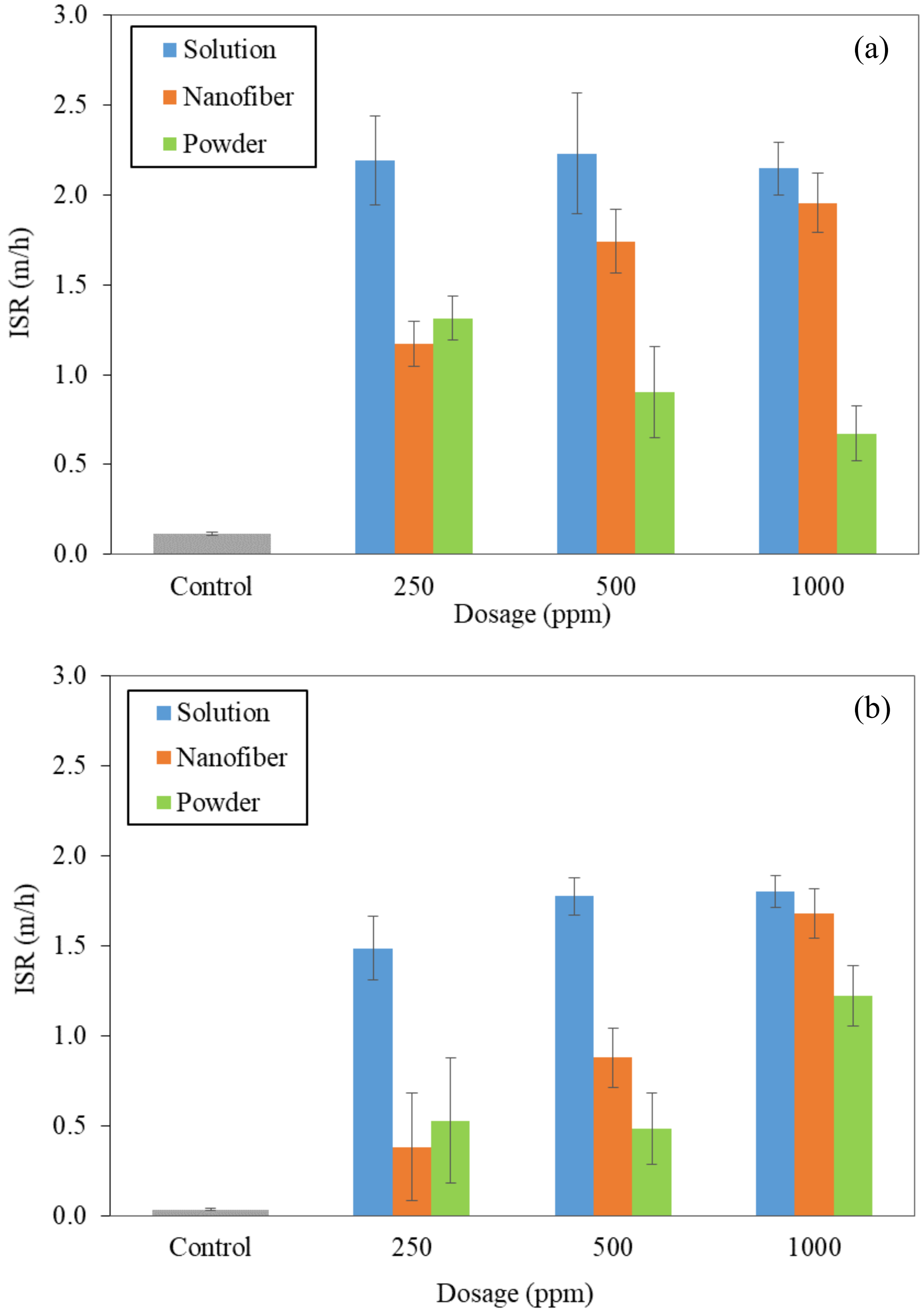

Figure 3.3. Initial settling rates (ISR, m/h) of kaolin flocculated with original polymer solution, polymer nanofiber and polymer powder at: (a) 5 wt. % kaolin loading, and (b) 10 wt. % kaolin loading.

3.3.3 Supernatant Turbidity

The turbidity of the supernatant after 24 h of settling of 5 wt. % and 10 wt. % kaolin is shown in Figures 3.4a and 3.4b, respectively. At 5 wt. % loading, both the nanofiber and the powder produce similar results in terms of supernatant clarity. Both forms of the polymer were able to capture clay particles with a wide size distribution when compared to the control. Additionally, as the polymer dosage increased, the turbidity remained comparatively unchanged. When the polymer solution was used, however, the water clarity decreased with increased dosage, suggesting that many fine particles remained suspended in the supernatant.

A similar trend was observed for 10 wt. % kaolin loading. As seen in Figure 3.4b, as polymer dosage increases, the supernatant turbidity increased when the suspension was treated with the polymer solution, while the turbidity of both nanofiber- and powder-dosed suspensions remained practically unchanged or increased slightly.

The clarity of the supernatant is mainly governed by the destabilization and subsequent bridging of negatively-charged clays in kaolin [119]. In all three forms, the DADMAC unit behaves as a polyelectrolyte, destabilizing particles by neutralizing charges on the negatively charged surfaces and bridging them together to yield clear supernatants at optimal dosages. The increase in supernatant turbidity with increasing polymer solution dosage may be attributed to steric and/or electrostatic repulsions between particles fully covered with the flocculant. Overdosing may promote interparticle repulsion due to the excess cationic charges (introduced by the polymer flocculant) on the flocs.

The supernatant contains particles that may be orders of magnitude smaller than those found in the original kaolin suspension creating a large difference in size distribution of clay. It may be speculated that nanofibers adsorb onto the clay surfaces more quickly than the polymer chains present in solution, allowing them to bridge the smaller particles in the kaolin suspension, while the polymer solution adsorbs preferentially onto larger particles, thus missing particles with smaller sizes that remained in the supernatant.

Interestingly, when comparing the control tests at each kaolin loading, 10 wt. % kaolin loading generated a supernatant that was less turbid than 5 wt. % kaolin loading. It is unknown at this time why this occurred. Due to the small size of the graduated cylinder and the increase of solids in the slurry, there could be an increase in van der Waals forces between the particles causing the kaolin to aggregate and settle more aggressively compared to the low solids loading case.

Conducting tests with 1 wt. % and 20 wt % kaolin may provide more insight into this observed phenomena.

As it can be seen in both cases of kaolin loading, the different forms of delivery of P(Am-*co*-DADMAC) produces turbidites that are statistically similar at lower dosages. While at higher dosages, both solid forms of the polymer are able to maintain a relatively unchanged level of turbidity when compared to the solution polymer. Both the settling rate and turbidity data show that there was little to no settling after 24 hours for the control tests.

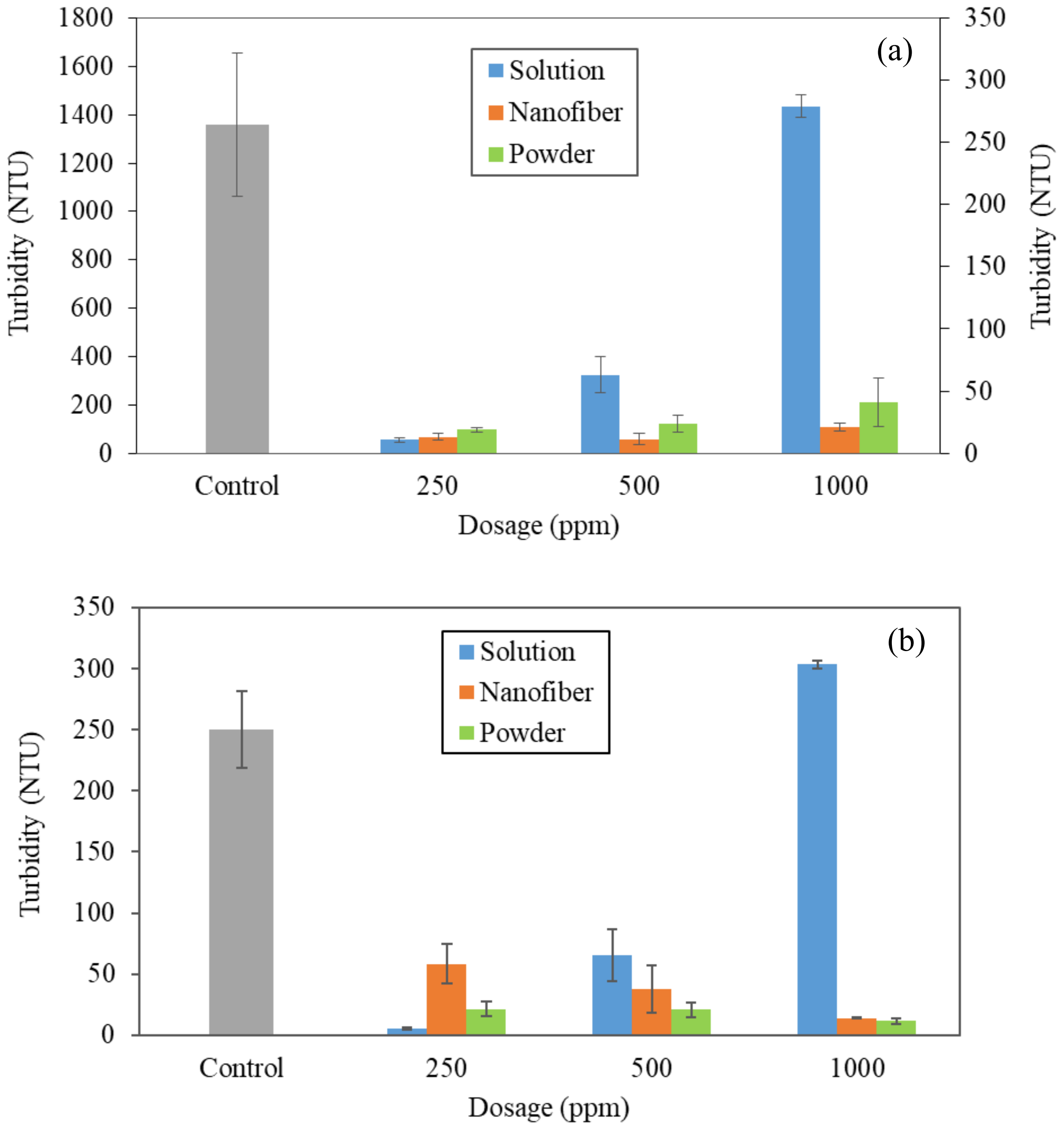

Figure 3.4. Turbidity (NTU) of kaolin flocculated with original polymer solution, polymer nanofiber and polymer powder at: (a) 5 wt. % kaolin loading with the control represented by the left y-axis and 250, 500 and 1000 ppm represented by the right y-axis, and (b) 10 wt. % kaolin loading.

3.3.4 Sediment Solids Content

The solids content of the sediment was determined after 24 h of settling. Figures 3.5a and 3.5b show solids content for 5 wt. % and 10 wt. % kaolin loading, respectively. As seen in Figure 3.5a, adding higher dosages of polymer show little to no effect on sediment solids content at 5 wt. % loading. In the case of 10 wt. % kaolin (Figure 3.5b), the polymer solution performs marginally better than the polymer nanofiber and powder at higher dosages.

Figure 3.6 compares kaolin sediments at 5 wt. % after 24 h of settling with polymer nanofiber and polymer solution (the supernatant was removed). The flocs produced by the nanofiber are visually larger than the ones produced by the polymer solution, which are more tightly packed and homogenized. Sediments produced with the polymer powder looked similar to those generated with the polymer nanofiber. In general, the effect of polymer addition on sediment consolidation is negligible, which may be due to the formation of big flocs and to the presence of significant amount of water trapped between particles [25]. To further improve the solids content of the sediments, other techniques such as filtration or centrifugation are required in this case.

Interestingly, in both kaolin loading cases, even though the turbidity of the supernatant of the control (natural gravitational settling) was much higher than the polymer treated kaolin, it also contained higher solids content which may be attributed to a dense, homogenized sediment bed that was formed after 24 hours of settling. The sediment bed may have made it easier for the water to be released while settling occurred. This may also explain the slight discrepancy between the solution polymer compared to the solid forms of the polymer. Since the flocs produced by the polymer solution are much smaller and more homogenized, it is less likely for water to be entrapped between flocs, which account for the slightly better performance of polymer solution at higher dosages. Additionally, recovering all of the kaolin sediment from the graduated cylinder after it was treated with polymer proved to be much more difficult compared to untreated kaolin. A small loss of sample may also contribute to the discrepancy of solids content between the control and polymer treated kaolin.

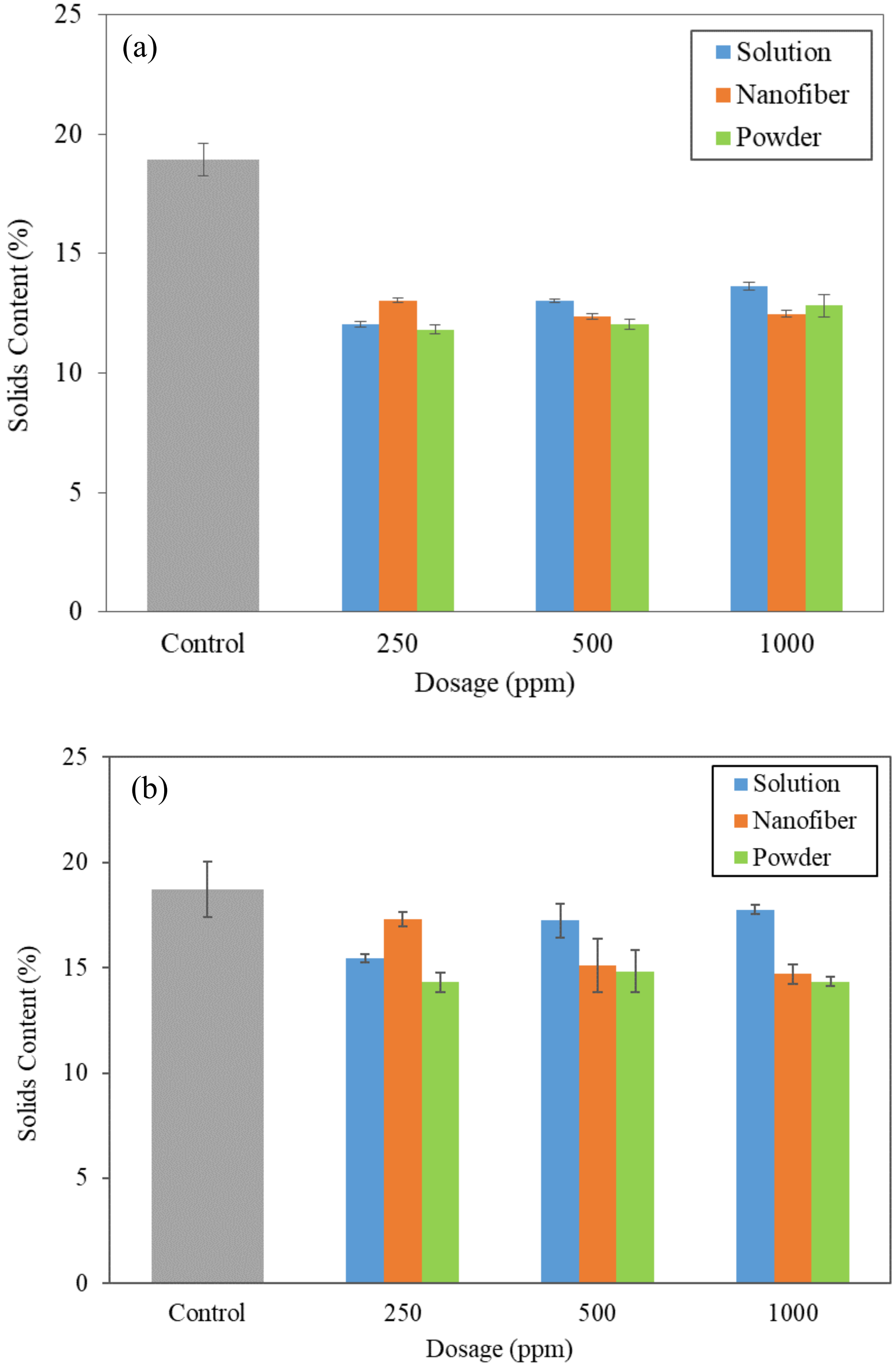

Figure 3.5. Solids content of kaolin flocculated with original polymer solution, polymer nanofiber and polymer powder at: (a) 5 wt. % kaolin loading, and (b) 10 wt. % kaolin loading.

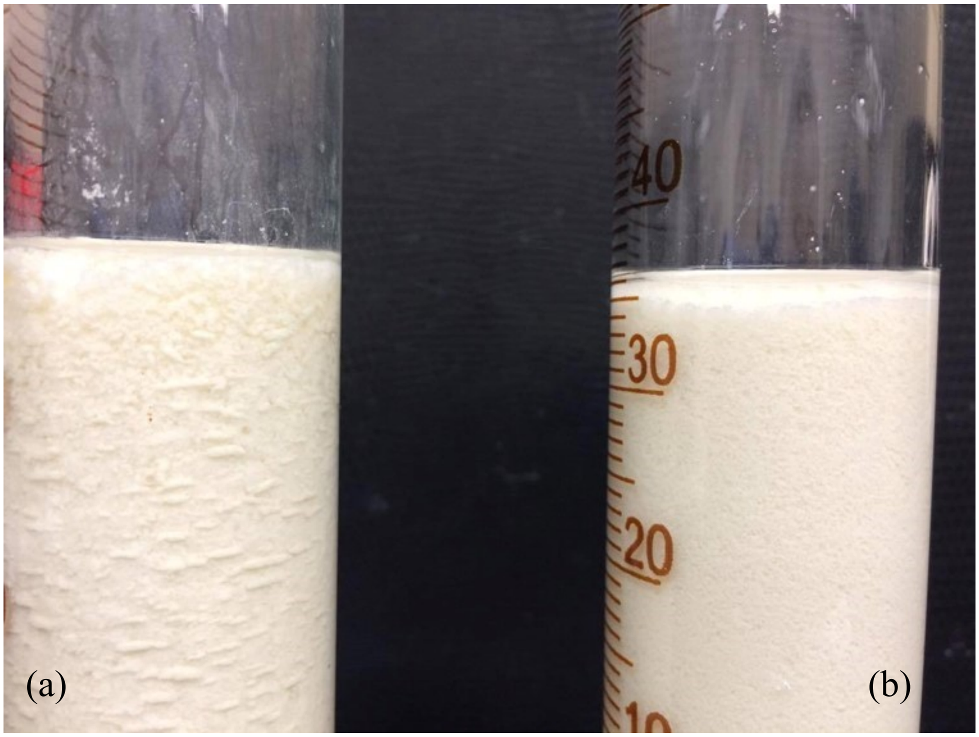

Figure 3.6. Sediment of 5 wt. % kaolin flocculated with 500 ppm of polymer nanofiber (a) and polymer solution (b) after 24 h of settling.

3.3.5 Water Recovery

Water recovery for 5 wt. % and 10 wt. % kaolin suspensions are contrasted in Figures 3.7a and 3.7b, respectively. The 5 wt. % kaolin suspension treated with each form of the polymer showed little change in water recovery as compared to the control. As the dosage of polymer increased, water recovery remained relatively constant, with each of the polymer forms displaying comparable effectiveness. The 10 wt. % kaolin suspension treated with polymer showed a little more variation of water recovery as compared to the control. As polymer dosage increased, the water recovery decreased slightly, with the polymer solution performing marginally better than the polymer nanofiber and powder at 1000 ppm. This is likely due to the size of the flocs produced by the nanofiber and powder. Since both formed larger flocs, it is likely that more water was trapped between these big flocs during the fast settling process, causing the loose sediment to decrease its solid content, when compared to the more homogenized sediment produced by the polymer solution. The trapped water can be easily recovered by filtration, but more so for 5 wt. % loading compared to 10 wt. % loading since there are less solids in the suspension.

Similar to the solids content study, the control was able to produce a significantly higher water recovery in both kaolin loading cases, while also producing high supernatant turbidity. These results are agreeable with the results of solids content; that is, clay suspensions with more solids in the sediment beds would correspond to more water being released into the supernatant. The high turbidity may be due the blank kaolin suspension not settling completely within 24 hours. Very fine particles are still left in the supernatant causing an increase in turbidity compared to kaolin treated with polymer which was able to settle much faster.

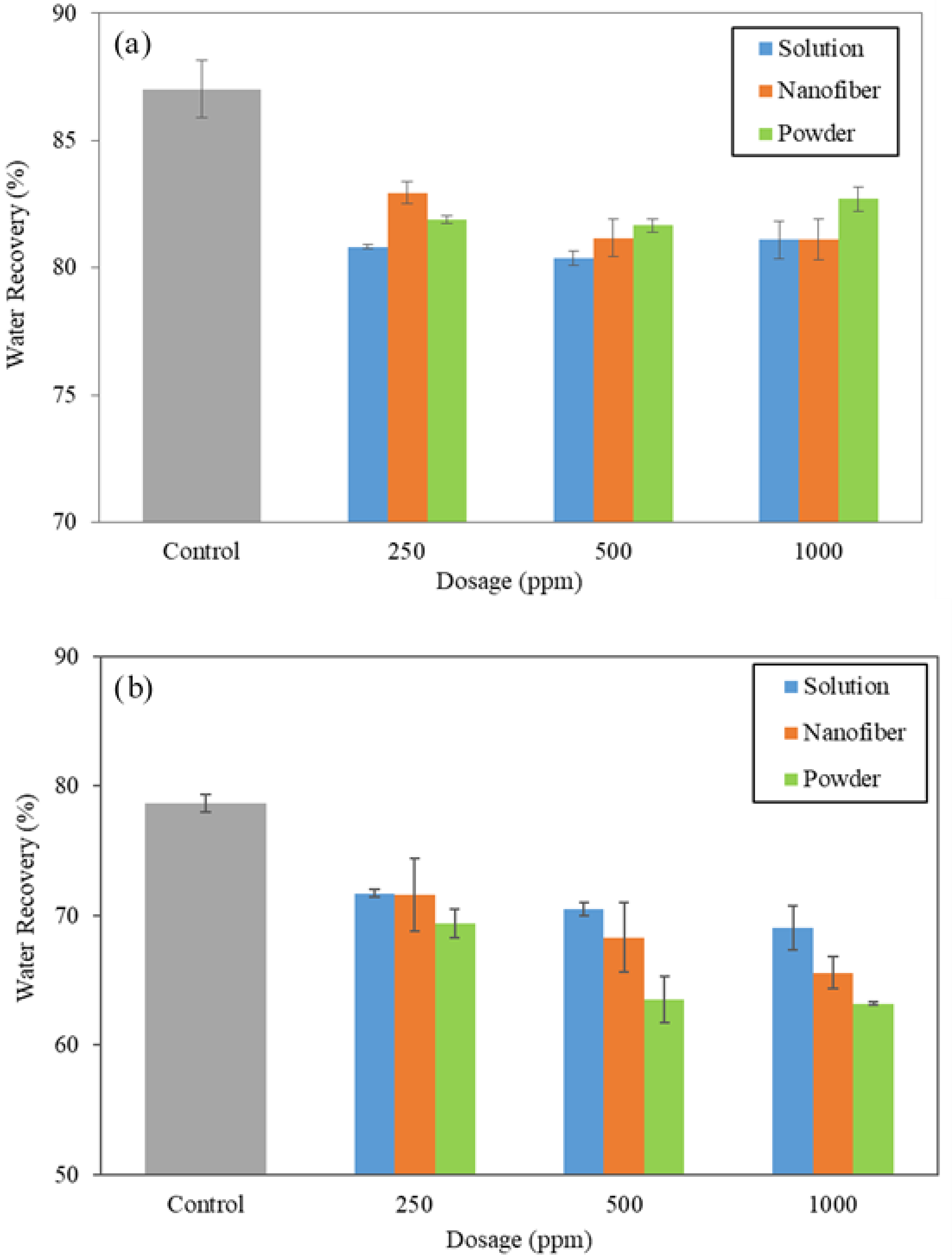

Figure 3.7. Water recovery of kaolin flocculate with original polymer solution, polymer nanofiber and polymer powder at: (a) 5 wt. % kaolin loading, and (b) 10 wt. % kaolin loading.

3.3.6 Dewaterability

Capillary suction time (CST) is a measure of the dewaterability of sludges which is often used to quantify the performance of flocculants [42]. The lower the CST that can be achieved, the more efficient the flocculant is at dewatering the sediments. Figure 3.8 shows the effect of polymer solution and nanofiber dosage on CST at 5 wt. % kaolin loading. Both the polymer solution and the nanofiber were able to achieve much smaller CSTs than the control case. When the dosage was increased, the CST of sediments flocculated with the nanofibers remained constant at approximately 6 seconds, while the CST of those obtained with the solution increased slightly from 6 seconds to 11 seconds. The difference may be due to the nanofibers forming denser flocs that were semi-open or nearly closed (low porosity), which reduced the diffusion of water into the flocs resulting in a lower CST. It appears that nanofibers can perform similar, if not better, than solution polymer in regard to dewaterability.

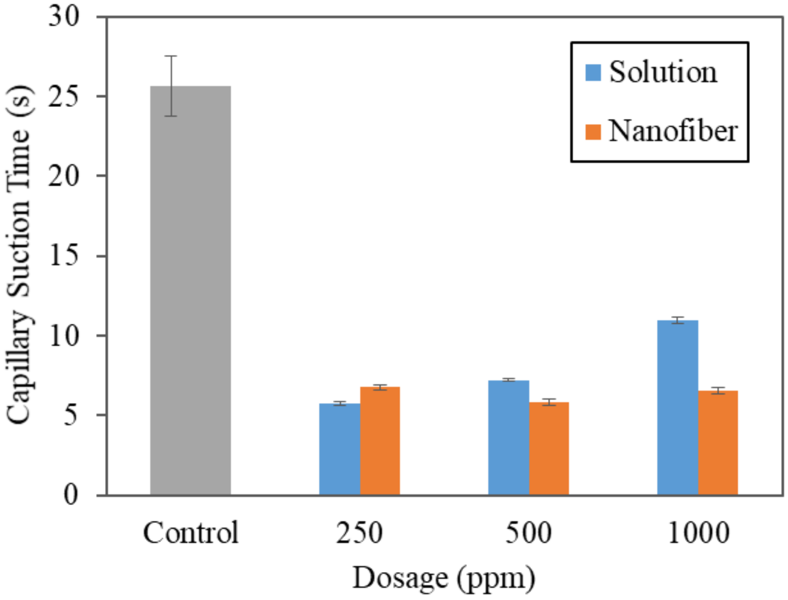

Figure 3.8. Capillary suction times for 5 wt. % kaolin with varying dosages of polymer solution and nanofiber.

3.3.7 Floc Formation

Figure 3.9a and 3.9b shows the real-time evolution of floc size in kaolin before and after the addition of 500 ppm of polymer solution and nanofiber, as measured by FBRM. Additionally, the time required to induce floc formation, floc stability, and change of average floc size over time can also be observed in these plots.

The kaolin suspension was mixed for 100 seconds at 300 rpm to ensure homogenization. Once it was determined that the kaolin suspension was homogenized and stable, polymer was added after 100 seconds, for both cases. The impeller speed was reduced to 150 rpm to ensure the flocs did not break during the test. It is evident from Figure 3.9 that the solution polymer took longer to disperse into the kaolin suspension and to adsorb onto the clay particles (approximately 30 s), while the nanofibers seem to instantly attach to the clay particles.

The time required for the adsorption of polymer chains onto particles, and subsequent floc formation, is called the characteristic adsorption time and is given by [54],

$$t_{ads} = \frac{-\ln(1-f)}{kN} \tag{3.3}$$

where f is the fraction of polymer needed to adsorb onto the clay surface and induce flocculation, k is the frequency of collision between polymer molecules and clay particles per unit time, and N is the initial number of particles in the kaolin suspension.

Figure 3.9b also shows that the nanofiber FBRM curve is slightly steeper, having a slope of 2.74 µm/s, compared to the solution curve, having a slope of 1.79 µm/s. The slopes of these curves are proportional to the rate of adsorption of P(Am-*co*-DADMAC) on the clay surfaces, leading to floc formation [54]. This indicates that not only does the nanofiber have shorter characteristic adsorption time, it also has a faster rate of adsorption onto clay particles. The average floc size of kaolin treated with polymer solution did not change as significantly as the kaolin treated with polymer nanofiber, as the average size of the particle size starts to decrease near the end of the flocculation period. This can be due to flocs breaking or to flocs becoming too heavy to stay suspended near the FBRM probe, thus going undetected. Since the impeller speed was reduced to ensure there was no floc breakup, it is likely that the decline in floc size was caused by the generation of large flocs that settled too quickly to be detected.

Figure 3.9 also shows that the nanofiber-treated kaolin has a break in the curve. The addition of nanofibers induced floc formation in kaolin and reached an intermediate stage where floc size remained constant for ~20 s and again increased to a maximum size of 80 µm. We speculate that the flocs underwent restructuring without the addition of particles that caused a further increase in floc size, which resulted in a steeper slope. However, a particular reason for such restructuring remained unknown during the course of this study. Advanced techniques such as atomic force microscopy (AFM) or utilizing a surface force apparatus (SFA) to examine the molecular phenomenon can be employed to investigate this behavior.

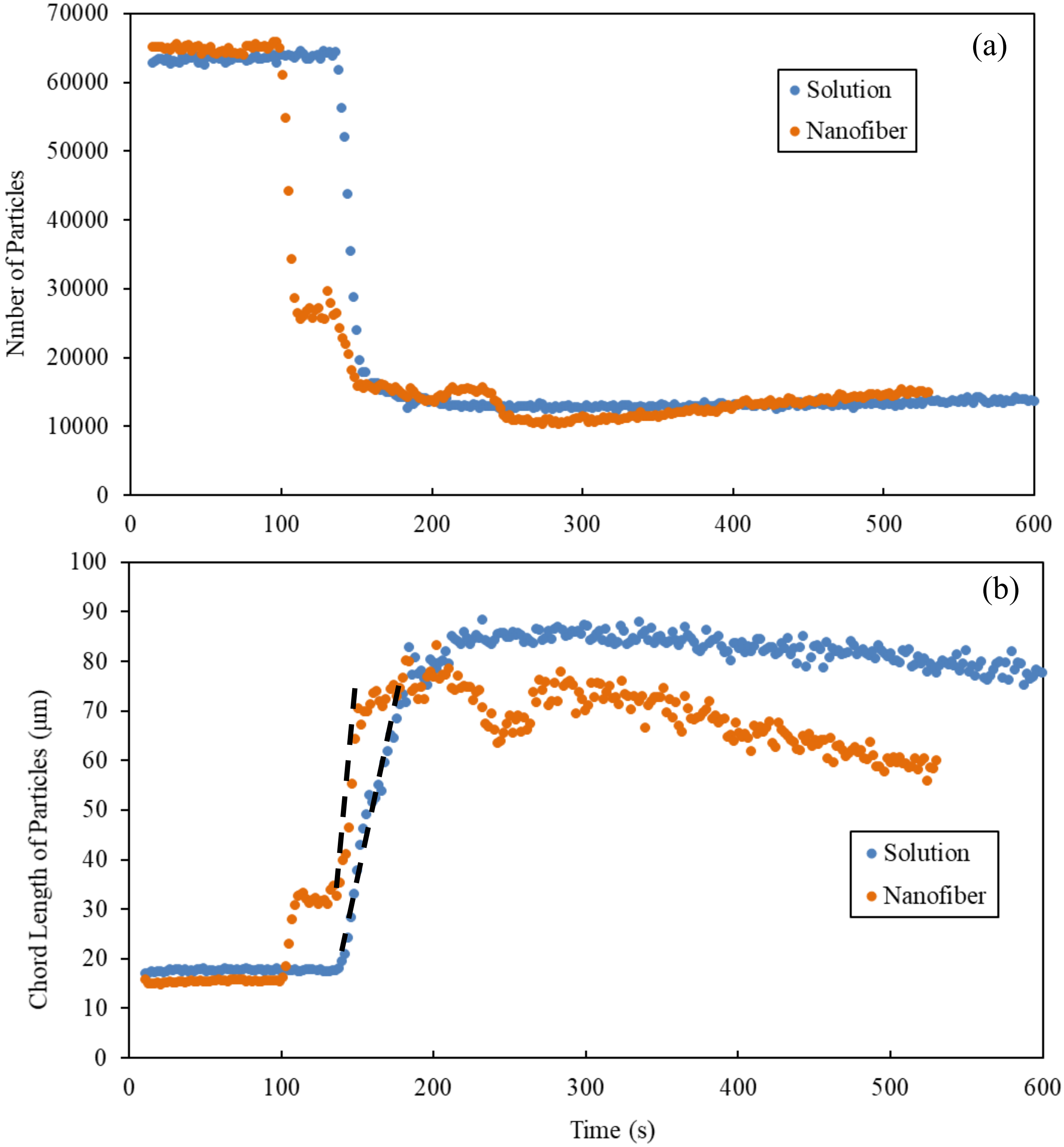

Figure 3.9. FBRM measurements for: (a) number of particles, and (b) chord length of flocs formed in kaolin using 500 ppm of polymer solution and nanofiber.

The average of 3 particle size distributions (PSD) for pure kaolin and for flocs produced with polymer solution and nanofiber are compared in Figure 3.10. Square weighted mean chord lengths were used because it resolves even small changes in floc size and represents an unbiased change in the system [129, 130]. It can be seen that the nanofiber treated kaolin is slightly shifted to higher average particle sizes. As mentioned before, the discrepancy in counts between nanofiber and solution may be due to large flocs settling faster and not being detected by the FPRM probe.

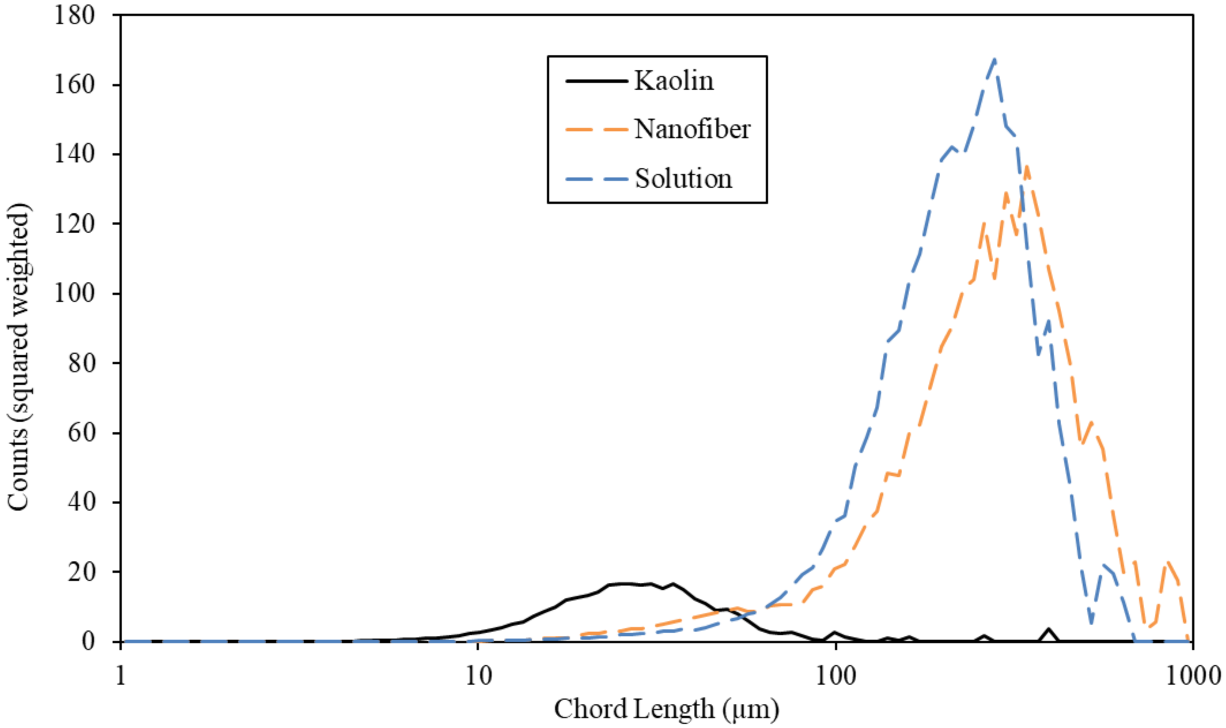

Figure 3.10 Floc size distribution of kaolin and kaolin flocculated with 500 ppm of P(Am-*co*-DADMAC) solution and nanofiber.

3.3.8 QCM-D

To understand the interactions between the different forms of P(Am-*co*-DADMAC) and kaolin, QCM-D was applied in real time. QCM-D technique has been used in the study of polymers and nanoparticles and their subsequent interactions [120 – 122]. In this work, each form of the polymer was immobilized on silica-coated sensor chips of the QCM-D. For simplicity and because kaolin is a layered silicate mineral [123], silica coated sensor chips were used to approximate P(Am-*co*-DADMAC) – kaolin interactions. It is important to note that kaolin is not pure silica (it also contains aluminum), therefore this study may not fully represent the adsorption behavior of P(Am-*co*-DADMAC) onto kaolin.

Desired dosages of polymers were first dissolved at different mixing times to understand how dissolution kinetics played a role in polymer adsorption. Each form of P(Am-*co*-DADMAC) was mixed for 1 min or 24 hours in DI water before being injected onto the silica sensor chips. The frequency shifts (of the 3rd overtone) as well as the change in mass and thickness of the polymer layer on the sensor after 1 minute and 24 hours of mixing are shown in Figures 3.11 and 3.12, respectively.

In Figure 3.11, among the three forms of polymers, the nanofiber-treated sensor exhibited the largest frequency shift and mass change, and hence the largest layer thickness after 1 minute of mixing. In Figure 3.12, as expected, all three treated sensors exhibited comparable frequency shifts and mass change after 24 hours of mixing. After 24 hours of mixing, all forms of the polymer are completely homogenized resulting in similar shifts. While comparing both mixing times, however, the difference of frequency shift and mass change between each form of the polymer is greater after mixing for 1 min compared to mixing for 24 hours. This could be due to the nanofibers having a larger surface area compared to the other forms allowing it to dissolve faster which would subsequently displace more mass onto the sensor.

It appears that through all three forms of the polymer, nanofibers are able to displace more mass on the silica chip in the same amount of dissolution time while the powder is able to displace similar, if not more, mass compared to the solution form.

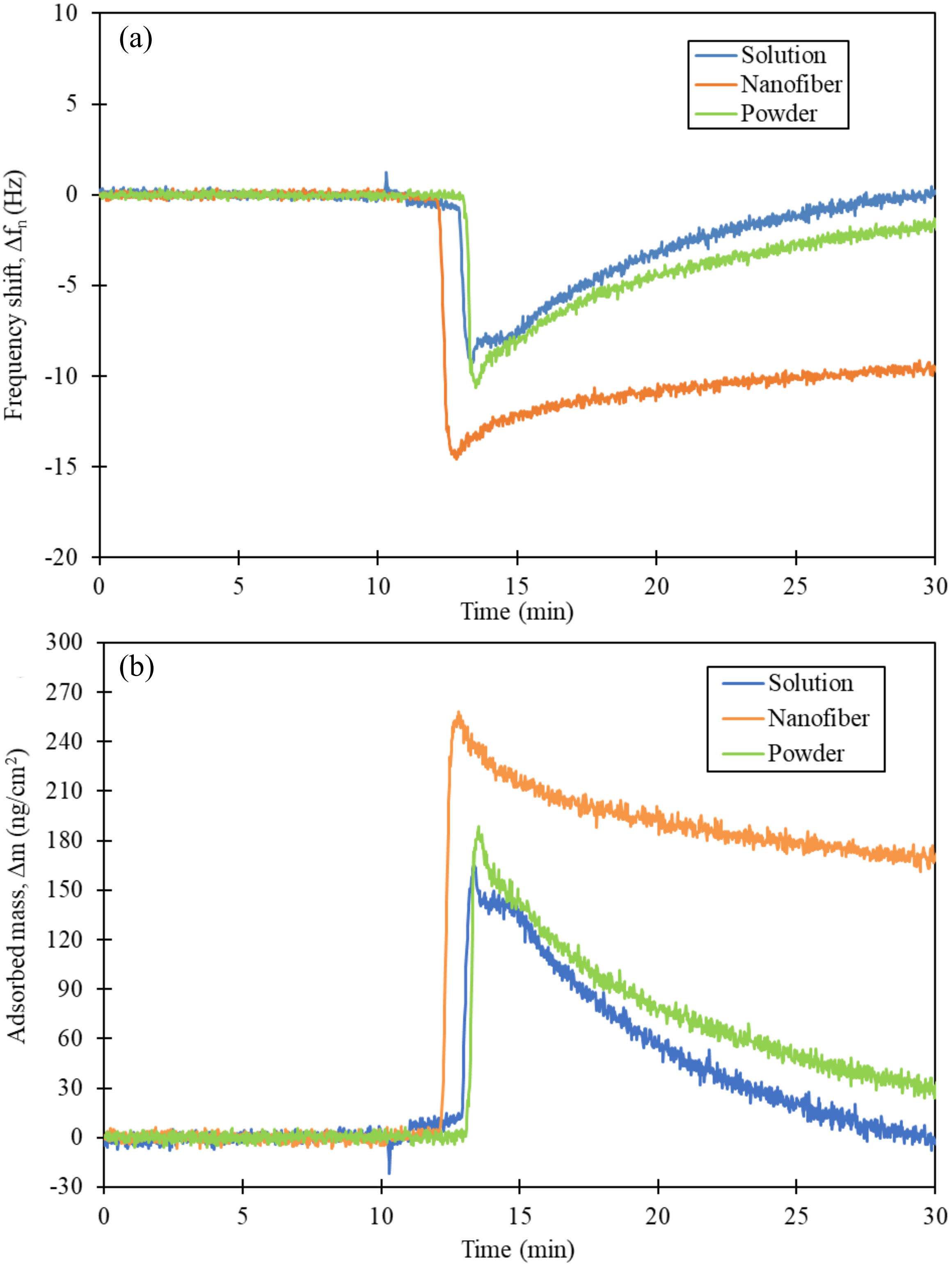

Figure 3.11. Frequency shift (a) and adsorbed mass (b) after 1000 ppm of polymer solution, nanofiber, and powder adsorbed on silica-coated QCM-D sensor chips. Polymers mixed with DI water for 1 min before injection.

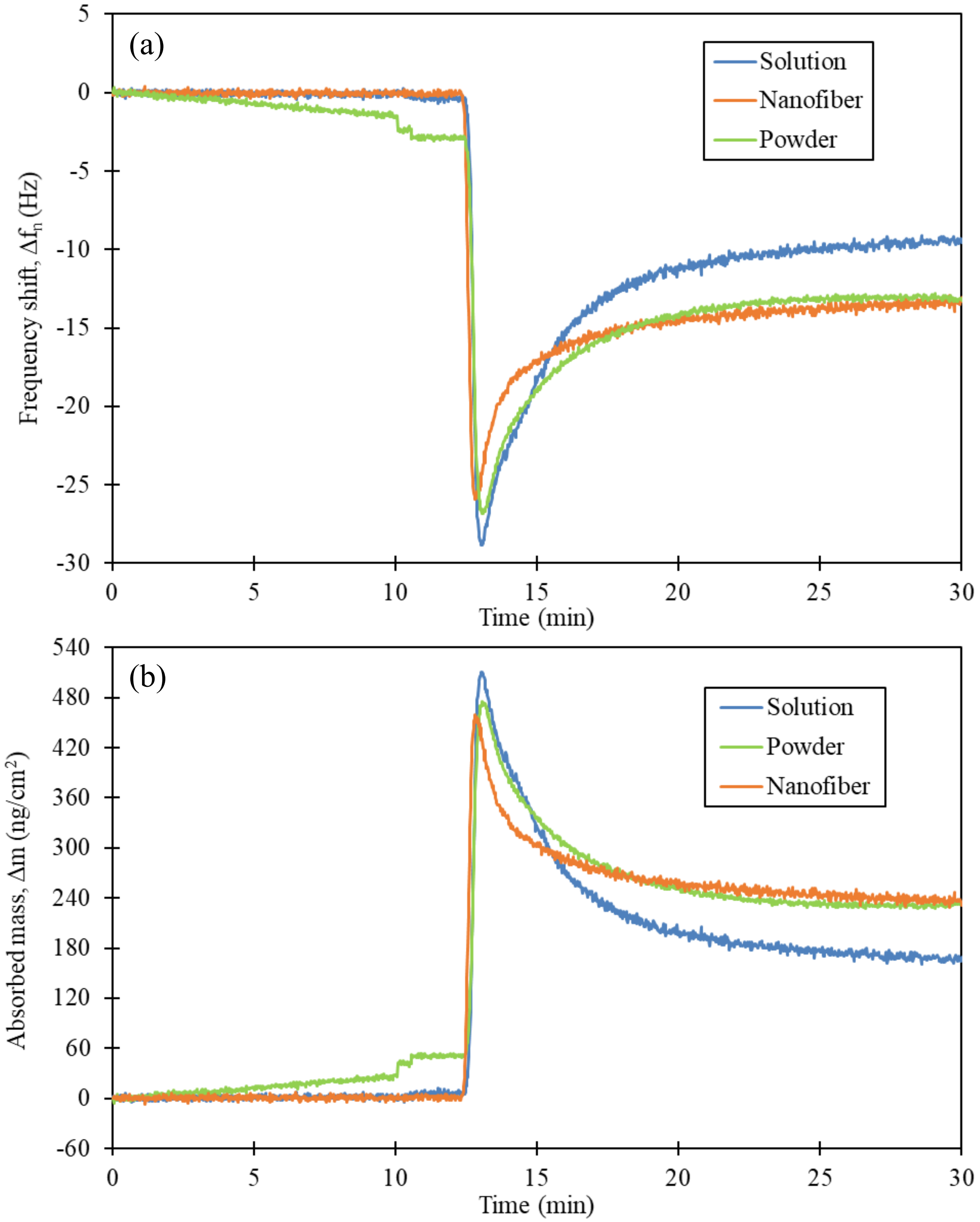

Figure 3.12. Frequency shift (a) and adsorbed mass (b) after 1000 ppm of polymer solution, nanofiber, and powder adsorbed on silica-coated QCM-D sensor chips. Polymers mixed with DI water for 24 h before injection.

3.4 Conclusion

In this study, we fabricated P(Am-*co*-DADMAC) nanofibers using bubble electrospinning for use as a novel flocculant for solid-liquid separation of mineral tailings. Nanofibers were compared with their original solution counterpart in different flocculation studies. The powder form of the polymer was also used as an additional control. The solid forms of the polymer required less mixing energy to be adequately dispersed in the suspensions, and also introduce savings in the water cost used in the flocculation process.

The initial settling rate (ISR) was higher for the P(Am-*co*-DADMAC) solution across all dosages at both 5 and 10 wt. % kaolin loadings, but the supernatant turbidity increased as the polymer dosage increased. However, the polymer solution showed signs of overdosing as its dosage increased. Nanofibers continuously improved ISR and clarity of the supernatant with increased dosages.

In practical applications, nanofibers are less sensitive to negative overdosing effects, minimizing the harmful consequences of potential dosing mistakes. At higher dosages, nanofibers achieved high ISR and low capillary suction times (CST), while also producing supernatants with high clarity, water recovery and solids content compared to polymer solutions.

Visually, nanofibers were able to produce larger flocs compared to the tightly packed, homogenized sediments produced with the polymer solution. Focused beam reflectance measurement (FBRM) studies showed that the rate of adsorption of P(Am-*co*-DADMAC) nanofibers onto the clay surface were slightly higher to that of P(Am-*co*-DADMAC) solution. Even though the P(Am-*co*-DADMAC) solution produced larger flocs, it took longer to form the flocs than when P(Am-*co*-DADMAC) nanofibers were used.

It was also determined through quartz crystal microbalance with dissipation (QCM-D) that the solid forms of the polymer were able to displace more mass onto the silica chip under similar dissolution times due to their larger surface area compared to the solution form of the polymer.

Nanofiber and polymer powder showed similar trends in most flocculation/dewatering tests, but the nanofibers were more efficient as a whole. These are promising initial results for a new class of flocculant.

Chapter 4 - Flocculation and Dewatering of Mature Fine Tailings

4.1 Introduction

As described in the last chapter, poly(acrylamide-*co*-diallyldimethylammonium chloride) nanofibers were generated by bubble electrospinning. The nanofibers, along with the original polymer solution used to produce the nanofibers, and poly(acrylamide-*co*-diallyldimethylammonium chloride) powder were used as flocculants to compare their dewatering efficiency in mature fine tailings (MFT). Flocculation studies included initial settling rate (ISR), turbidity, water recovery, solids content, sediment dewaterability. Results show that there are differences in effectiveness between all three forms of poly(acrylamide-*co*-diallyldimethylammonium chloride), suggesting that a new form of flocculant for the treatment of mineral tailings may be derived from this innovative concept.

4.2 Materials and methods

4.2.1 Materials

Poly(acrylamide-*co*-diallyldimethylammonium chloride) solution P(Am-*co*-DADMAC) and surfactant Triton X-100 were purchased from Sigma-Aldrich Chemicals (Oakville, ON, Canada). Imperial Oil (Fort McMurray, AB, Canada) provided the MFT samples used in our investigation. Polymer nanofibers and powder were produced and characterized the same way as described in Chapter 3.

4.2.2 MFT Characterization

Table 4.1 shows the composition of solids water, and bitumen in the MFT sample determined by Dean-Stark extraction [124]. Concentrations of major ions in MFT were measured by atomic adsorption spectroscopy (Varian 220FS), as shown in Table 4.2. The MFT used in flocculation tests in this work was the same as that characterized by Thompson et al. [125].

Table 4.1. Composition of mature fine tailings

Compound	Wt. %
Bitumen	4.2
Solids	32.3
Water	62.7

Table 4.2. Composition of ion in mature fine tailings

Ion	Quantity (ppm)
Mg^{2+}	12.4
K^{+}	17.3
Ca^{2+}	25.6
Na^{+}	251.6

4.2.3 Settling Tests

In this study, dewatering tests included initial settling rate, turbidity of supernatant, water recovery, solids content, and capillary suction time (CST). Nanofiber and polymer dosages ranged from 1000 – 5000 ppm. To begin each set of tests, 300 mL of MFT suspension of 5 wt. % solids was prepared by diluting 33 wt. % MFT with deionized water. The MFT suspension was first mixed at 600 rpm using a 45º pitch blade turbine impeller with four blades (4.8 cm in diameter) for 2 min to ensure homogenization.

Two different procedures were followed, depending on whether polymer nanofiber/powder or solution was added to the MFT suspension. In the case of nanofibers and powder, the desired dosage of polymer was placed in an empty graduated cylinder. The MFT suspension was then added to the cylinder until a volume of 100 mL was reached. In the case of the polymer solution, a second stage of mixing was required. After the first stage of mixing, the desired amount of polymer solution was added dropwise to the MFT solution and mixed for additional 2 min. The mixing rate was then reduced to 200 rpm, and the suspension was mixed for additional 8 min.

An aliquot (~5 mL) of this suspension was taken for capillary suction time measurements. The remaining mixture was then transferred to 100 mL graduated cylinder. In both cases, the cylinder was then inverted 5 times and then left still at room temperature. The height of the mudline (interface of supernatant and sediment) was recorded as a function of time. The sediment was left to settle for 24 hours. Initial settling rate (ISR), turbidity of supernatant, water recovery, solids content, and capillary suction time (CST) were measured in similar fashion as described in Chapter 3.

4.3 Results and Discussion

4.3.1 Initial Settling Rate (ISR)

Figure 4.1 compares initial settling rates of 5 wt. % MFT treated with the different forms of P(Am-*co*-DADMAC) at three different dosages (1000, 2500 and 5000 ppm). The floc formation process involves neutralizing the negative charges on the clay surfaces with the cationic charges found in DADMAC, and then bridging the clay particles as the adsorbed polymer segments attach to the bare surfaces of other colliding clay particles.

Figure 4.1 shows that the polymer nanofiber, powder and solution experience overdosing because as the polymer dosage increases, the initial settling rate decreases. Additionally, MFT suspensions treated with polymer nanofibers had the largest ISR at lower dosages. This may be due to an increase in positive charge and free energy on the polymer surface due to the bubble electrospinning process [126, 127]. Surprisingly, both powder and nanofibers always outperform the polymer solution, which may be related to the dissolution kinetics of these materials. The dissolution of a polymer generally occurs in two steps. Initially, the polymer swells as it adsorbs the solvent molecules that are diffusing through the polymer matrix. The polymer slowly breaks down allowing the molecules to disperse in solution [128]. The hydrodynamic radius of polymers dissolved in solvent are in the magnitude of a few nanometers. In this study, the polymer in the solution form is already fully dissolved in water before being introduced to the MFT slurry. However, nanofibers and powders are much larger when first introduced directly to a solvent and could have a hydrodynamic radius in the magnitude of micrometers when going through the first step of dissolution. The initial interactions of the nanofibers or powder with MFT may be able to bridge more particles, increasing their settling rate.

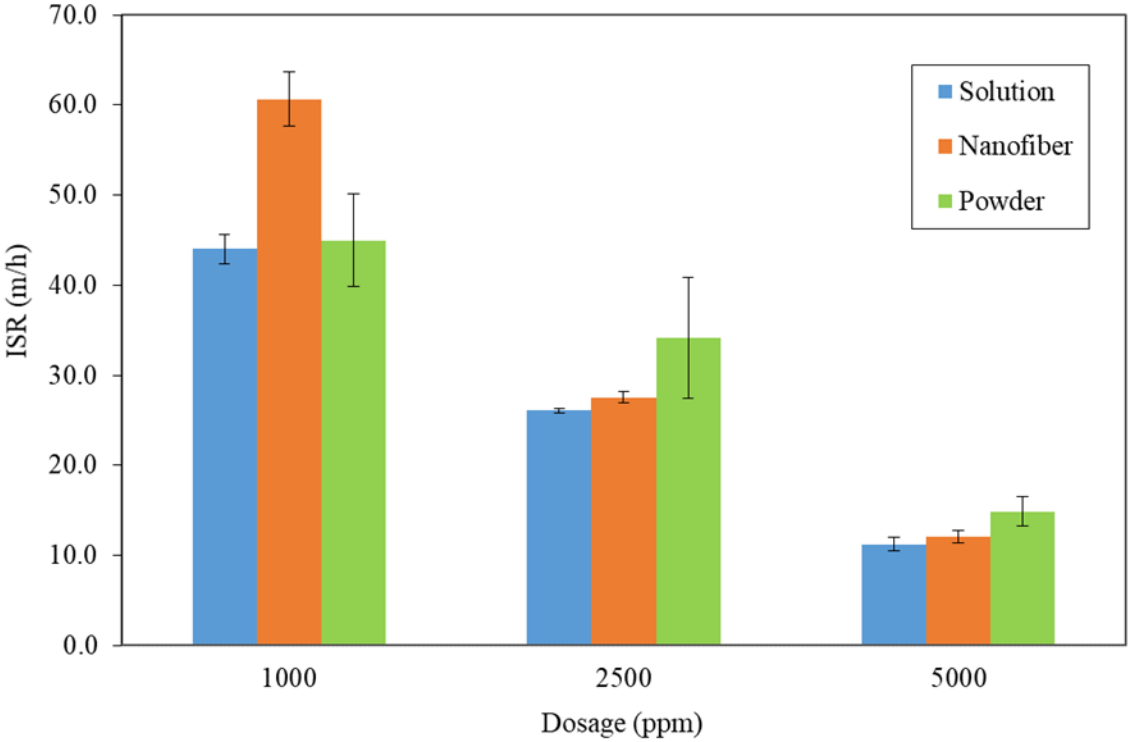

Figure 4.1. Initial settling rates (ISR, m/h) of 5 wt. % MFT flocculated with original polymer solution, polymer nanofiber and polymer powder.

4.3.2 Supernatant Turbidity

The turbidity of the supernatant after 24 h of settling of the 5 wt. % MFT suspension is shown in Figure 4.2. All polymer forms show similar trends. All forms could capture clay particles with a wide size distribution at 1000 ppm. Nanofibers performed marginally better throughout each dosage, which may be due to an increase in cation density at the surface of the nanofibers which allows for more effective charge neutralization. The clarity of the supernatant is mainly governed by the destabilization and subsequent bridging of negatively-charged clays in MFT. In all three forms of the polymer, DADMAC behaves as a polyelectrolyte, destabilizing particles by neutralizing the charges on the negatively charged surfaces and bridging them together to yield clear supernatants at optimal dosages. However, the increased supernatant turbidity with increasing polymer solution dosage can be attributed to steric and/or electrostatic repulsions. Overdosing, resulting in too much coverage of polymer on solids, can cause interparticle repulsion forces introduced from the exceeding accumulated cationic charges present on the flocs. The supernatant contains particles smaller than particles found in the original MFT suspension creating a large difference in the size distribution of clay. Solid forms of the polymer may adsorb onto fines more quickly than the polymer solution allowing it to bridge smaller particles in both the MFT suspension and supernatant.

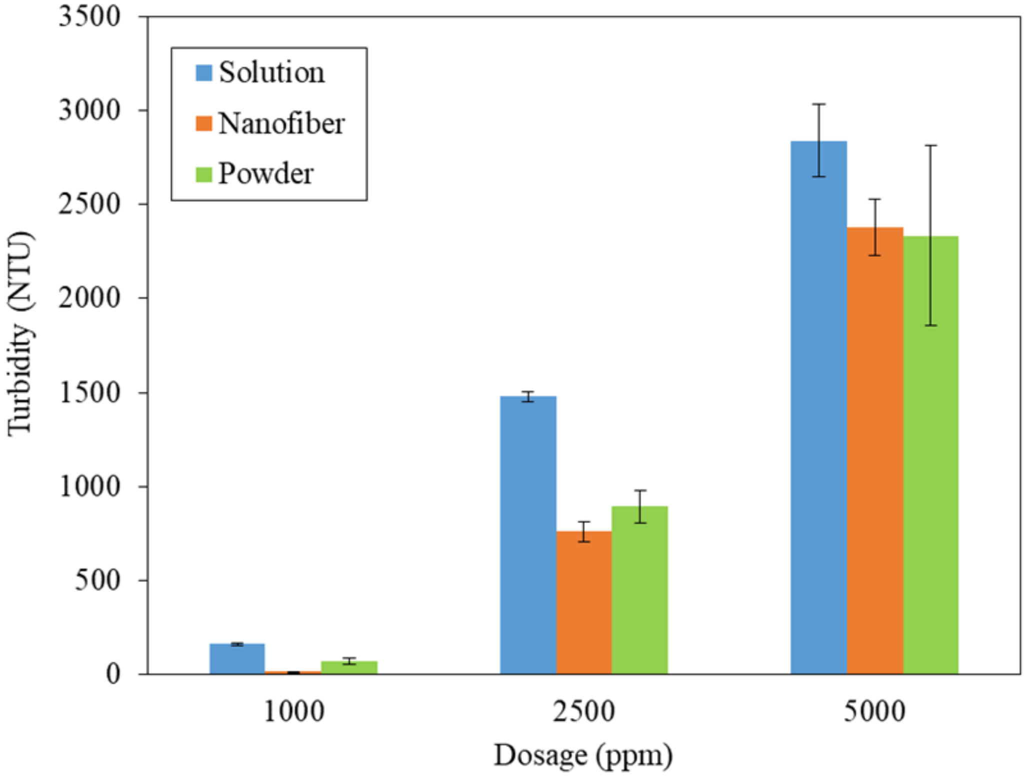

Figure 4.2. Turbidity (NTU) of 5 wt. % MFT flocculated with original polymer solution, polymer nanofiber and polymer powder.

4.3.3 Sediment Solids Content

The solids content of sediment was determined after 24 h of settling. Figure 4.3 shows the solids content for 5 wt. % MFT. As shown in Figure 4.3, adding higher polymer dosages does not increase the sediment solids content significantly. Nevertheless, nanofibers start to perform better at higher dosages compared to the polymer solution. Unfortunately, the trade off between increased solids content and decreased ISR and supernatant clarity is not desirable. Figure 4.3 also shows the polymer solution performs marginally better than the polymer nanofiber and powder at lower dosages. The poorer nanofiber performance at the lower dosages may be due to the formation of big flocs that trap more water. Although an increase in dosage can increase solids content, settling rate and turbidity of the supernatant will be sacrificed through all deliveries of polymer.

Figure 4.4 and Figure 4.5 show the sediments generated after the flocculation of 5 and 33 wt. % MFT with 1000 ppm of nanofiber and polymer solution, respectively. For the 5 wt. % MFT, the sediment was left to settle for 1 hour after the mixing stage(s) of polymer nanofiber and solution, while the 33 wt. % MFT was left to settle for 24 hours. Figure 4.4 shows that the flocs produced by the nanofiber are larger than the ones produced by the polymer solution, which seem to be more tightly packed and homogenized. The polymer powder generates sediments with that similar to those obtained with the polymer nanofiber (not shown in Figure 4.4 or Figure 4.5).

Figure 4.5 shows that, with respect to the large (undiluted) MFT loading, nanofibers produce channels for water to escape even at a very low dosage, while the polymer solution is unable to settle the solids. This is demonstrated by the complete coverage of MFT by the polymer solution and lack of supernatant in the graduated cylinder. In general, the effect of polymer addition on sediment consolidation is negligible, which may be due to the formation of big flocs and due to the presence of significant amounts of water trapped between particles. As with kaolin, to further improve sediment solid content, other techniques such as filtration and centrifugation are required.

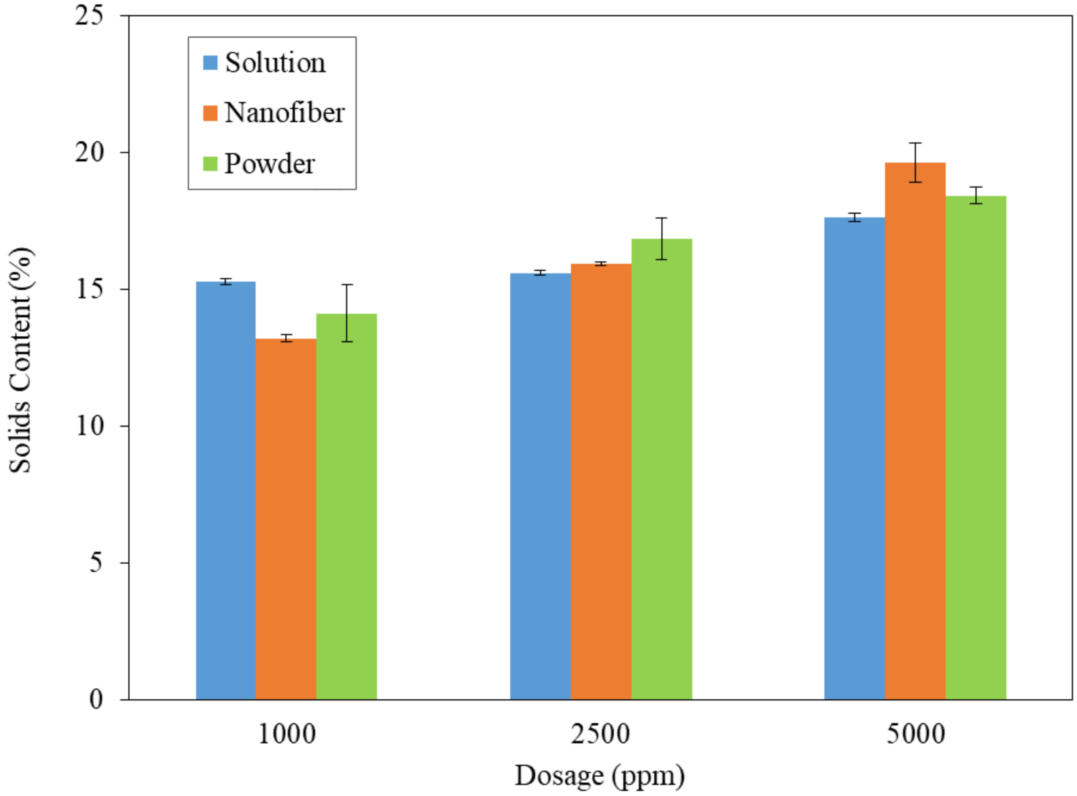

Figure 4.3. Solids content of 5 wt. % MFT flocculated with original polymer solution, polymer nanofiber and polymer powder.

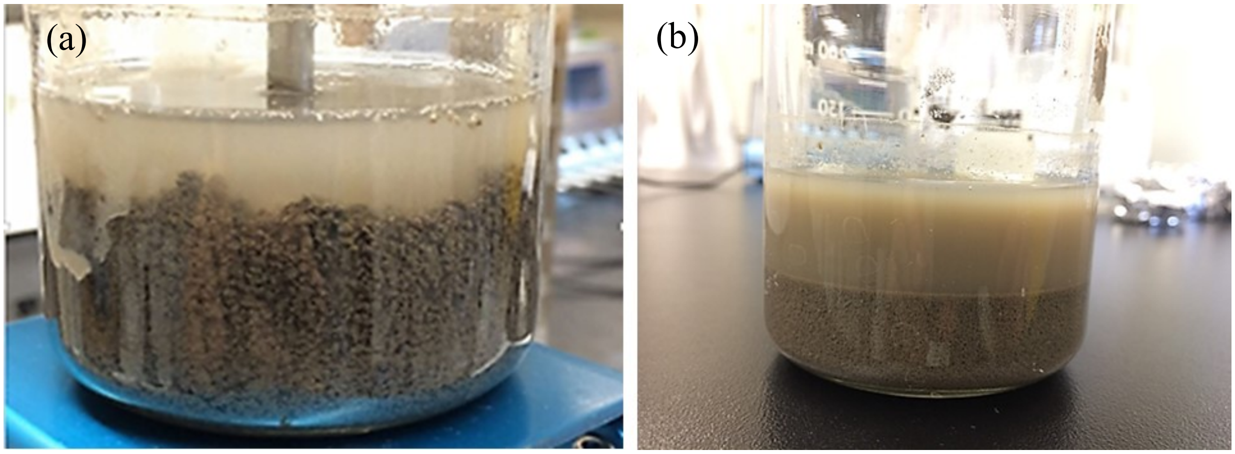

Figure 4.4. Sediment of 5 wt. % MFT flocculated with 1000 ppm of polymer nanofiber (a) and polymer solution (b) after 1 hour of settling.

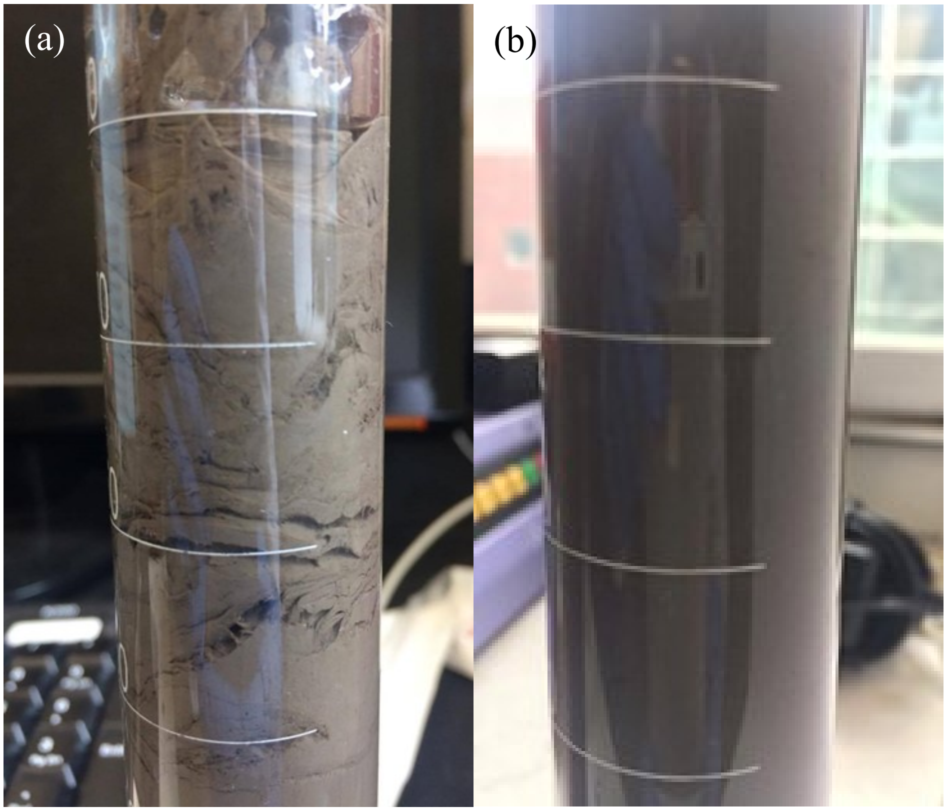

Figure 4.5. Sediment of 33 wt. % MFT flocculated with 1000 ppm of polymer nanofiber (a) and polymer solution (b) after 24 hours of settling.

4.3.4 Water Recovery

The water recovery results of 5 wt. % MFT suspensions are compared in Figure 4.6. The 5 wt. % MFT suspension treated with each form of the polymer showed little change in water recovery throughout each dosage. As the dosage of polymer increased, water recovery decreased slightly from approximately 78% to 68% with each of the polymer forms displaying comparable effectiveness. Again, the decrease in performance seems to be due to polymer overdosing. It seems that more water being trapped in the flocs as the polymer dosage is increased, but it is conceivable that this water may be easily recovered by filtration or centrifugation processes.

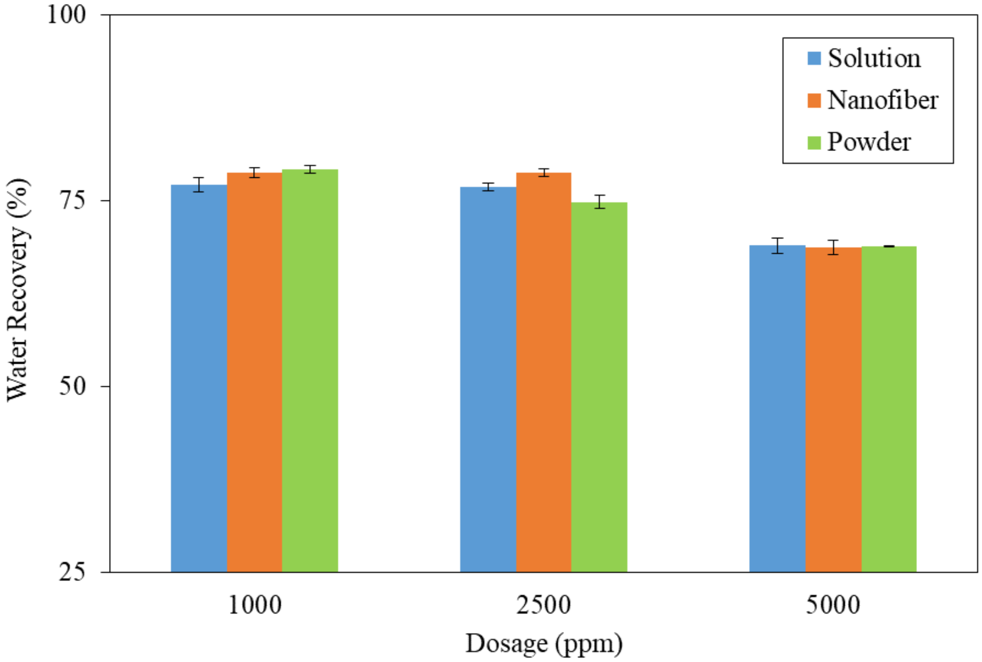

Figure 4.6. Water recovery of 5 wt. % MFT flocculated with original polymer solution, polymer nanofiber and polymer powder.

4.3.5 Dewaterability

Capillary suction time (CST) is a measure of the dewaterability of sludges, which is often used to quantify the performance of flocculants. The lower the CST that can be achieved, the more efficient the flocculant is at dewatering a suspension.

Figure 4.7 shows the effect of polymer solution, nanofiber, and powder dosage on CST at 5 wt. % MFT. All forms of the polymer were able to achieve a CST at a fraction of what natural settling could achieve, with pure MFT having a CST higher than 300 seconds [54]. In the oil sands industry, CST values less than 20 seconds are acceptable. As with every other test, the powder performs similar or marginally better than the polymer solution. With increasing dosage, the CST of the nanofibers increased slightly from 5 seconds to 30 seconds while the CST of the solution and powder increased greatly from 6 seconds to 75 seconds. Overdosing does not affect nanofibers as significantly in terms of how quickly water is released from sediments compared to polymer solution and powder. The difference may be due to the nanofibers forming denser flocs that were semi-open or nearly closed (low porosity), which reduced the diffusion of water into the flocs resulting in a lower CST.

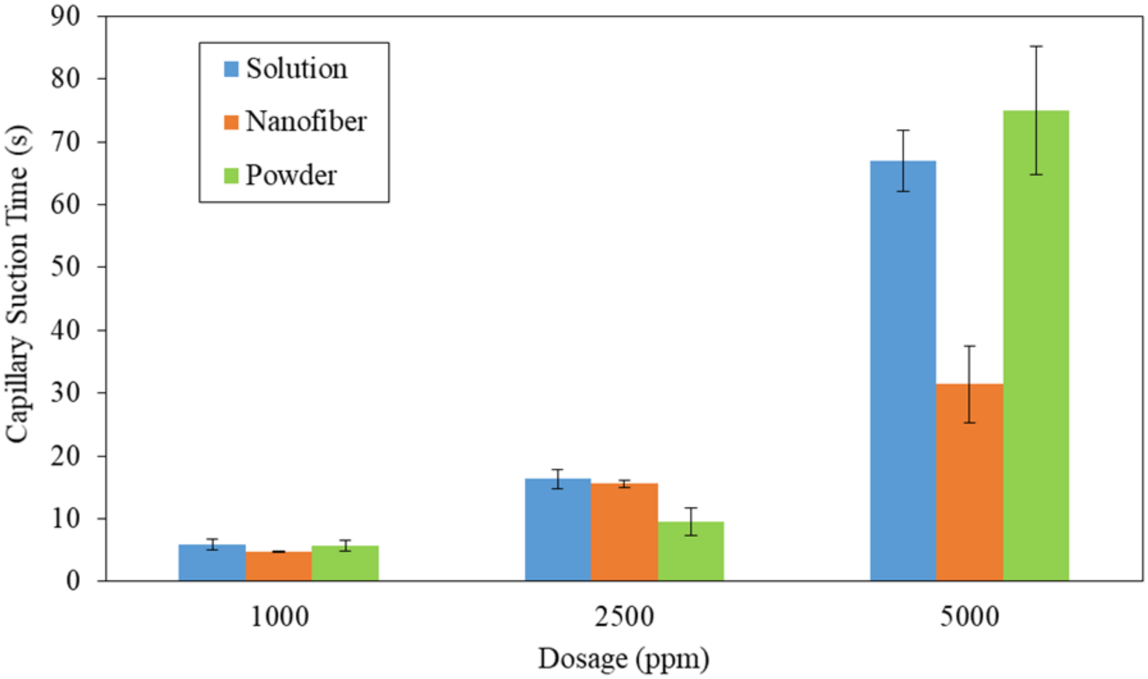

Figure 4.7. Capillary suction times for 5 wt. % MFT treated with different dosages of polymer solution, nanofiber and powder.

4.4 Conclusion

In this study, P(Am-*co*-DADMAC) nanofibers were fabricated and used as a novel flocculant for solid-liquid separation of MFT suspensions. Nanofibers were compared with their original solution counterpart as well as their powder, to find out whether the difference in physical properties of the nanofibers and powder had any influence on the flocculation procedure.

The initial settling rate (ISR) of a 5 wt% MFT suspension was higher for P(Am-*co*-DADMAC) nanofiber at a dosage of 1000 than for the polymer solution and powder, which behaved similarly. All three polymer forms showed signs of overdosing as the polymer dosage increased over 1000 ppm, as shown by a decrease in ISR, and increase in supernatant turbidity and CST.

From a practical standpoint, nanofibers have advantages over polymer solutions because nanofibers were less sensitive to overdosing in terms of CST, minimizing the harmful effects of potential mistakes in dosage. Additionally, the use of nanofibers and powders eliminates the need to dilute or create a polymer stock solution with excess water at desired dosages. At lower dosages, solid forms of polymer can achieve high or similar ISR and low capillary suction time (CST), while also delivering high clarity in the supernatant and comparable water recovery and solids content compared to the equivalent polymer solution. Visually, polymer nanofibers and powders produced much larger flocs than the tightly packed, homogenized sediment produced with the polymer solution.

It was expected that after each form of the polymer was dissolved in the medium, each form of the polymer would perform equally in each test. However, throughout each test, especially at lower dosages of polymer, the powder and nanofibers were able to perform similar or marginally better than the polymer solution, which also presents advantages with respect to how polymers are introduced into MFT treatment systems. The solid forms of the polymer, either as nanofiber or a powder, require less mixing energy to be adequately dispersed in suspensions, as well as introduce a savings in water cost used in the flocculation process.

Chapter 5 - Conclusions and Future Work

Water soluble polymeric nanofibers were fabricated from commercial P(Am-*co*-DADMAC) solution in larger quantities than previously possible with traditional needle electrospinning via bubble electrospinning. The subsequent fibers were used as a flocculant for kaolin suspensions and MFT.

The flocculation performance of the nanofibers was compared to that of the equivalent polymer solution and polymer powder, which acted as controls. These comparative experiments were designed to help find out whether the particular morphology of the nanofiber had any influence on the flocculation process.

The flocculation efficiency for the kaolin suspensions and MFT was investigated through five performance measurements: initial settling rate, turbidity, solids content, water recovery, and dewaterability. In addition, the cleaner kaolin suspensions also allowed for the use of quartz micro balance and focused beam reflectance measurement, to further understand the flocculation mechanism with polymer nanofiber, powder and solution.

Fourier transform infrared spectra analysis and size exclusion chromatography fractionation showed that there was no change in polymer composition or molecular weight when the commercial polymer was put through the energy intensive electrospinning process. All three forms of the polymer had similar chemical composition and molecular weight.

The kaolin studies showed that polymer nanofiber, powder, and solution performed similarly with respect to ISR, solids content, and water recovery at optimum dosages. However, the solid forms of the polymer (powder and nanofiber) maintained high supernatant clarity with increasing dosages, while the polymer solution did not. Although both solid forms of the polymer behave in a similar manner due to their large surface area, a possible increase in surface charge on the nanofibers as a result of bubble electrospinning can neutralize finer charged particles and enhance the polymer adsorption onto particles, while the higher surface area to volume ratio allows for initial, strong interactions between nanofibers and kaolin particles allowing for rapid flocculation and dewatering that caused the nanofiber to perform slightly better than the powder. Similar trends were observed for 5 and 10 wt. % kaolin loading.

Moreover, polymer nanofiber and powder formed larger flocs than those generated by the polymer solution, which were smaller and more homogenized. QCM-D and FBRM results showed that the dissolution kinetics of nanofibers may play a role in flocculation efficiency. Polymer nanofibers were able to adsorb onto clay surface and produce flocs more quickly when compared to the polymer solution, perhaps due to their larger surface area to volume ratio and initial interaction with clay particles when first introduced to the kaolin system.

MFT studies displayed similar results in terms of sediment formation. Both sediments treated with the solid forms of the polymer contained larger flocs while the solution polymer produced tightly packed and homogenized flocs. Apart from sediment formation, water recovery and solids content remained relatively constant and increased, respectively, as polymer dosage was increased. Additionally, at the low dosages, nanofibers achieved high ISR, low turbidity, and high dewaterability when compared to the polymer solution and powder. Akin to studies done with kaolin, the possible increase in cationic surface charge caused by the bubble electrospinning process, as well as the dissolution kinetics, played an important role in the flocculation efficiency of the nanofibers. It is also important to note that the polymer powder performed as well as, if not better, then the polymer solution across all tests and dosages.

Kaolin was used in this study to simulate and simplify the MFT system to easily understand the mechanisms behind flocculation behavior using polymer nanofibers and powder. Interestingly, the kaolin tests imply little to nothing about how well these flocculants would work in a much more complex environment such as MFT. For example, based on initial settling rate, it appears that polymer powders would not be ideal when used as a flocculant when compared to polymer solution. However, when used in MFT, polymer powders perform similar or better than polymer solutions. The same can be seen for nanofibers. While they did not perform as well in kaolin compared to polymer solution, they were able to outperform the solution in MFT by a large margin at a low polymer dosage. It is important to understand that these systems behave very differently, and results from a simpler case may not fully represent or can even misrepresent more complex systems.

The advantages of polymer nanofibers and powders are that they would allow for less water consumption and mixing energy when introduced into mature fine tailings. Additionally, they would reduce the damage caused by overdosing because of their robustness. However, powders are much easier and cheaper to produce compared to nanofibers. That being said, nanofibers show promising initial results to efficiently dewater MFT when compared to their polymer solution counterpart, although further investigation is required to make them commercially competitive.

A few lines for future study are proposed below:

1. Gradually increase the solid weight percent of MFT used in flocculation tests from 5 wt. % to loadings closer to undiluted MFT (~33 wt. %) with a larger range of polymer dosage.
2. Measure polymer nanofiber and powder dissolution kinetics and floc formation during the flocculation of MFT.
3. Determine how consolidated sediment properties after flocculation, such as sheer strength, are affected by the use of the same polymer in solution, powder, or nanofiber forms.
4. Use mechanical techniques (filtration, centrifugation, thermal drying, electrical treatment and freeze thaw treatment) in conjunction with polymer nanofiber, powder and solution to find out how much more water can be recovered from the sediments as a function of the polymer form.
5. Change system parameters to further replicate industrial environments in northern Alberta such as flocculating at lower temperatures and using process water instead of deionized water.
6. Repeat these analyses with different types of water-soluble polymers to find out if general trends are observed when solutions, powders, and nanofibers of the same polymer are compared.

Bibliography

[1] Government of Alberta - How the royalty system encourages environmental responsibility. https://www.alberta.ca/royalty-encouraging-environmental-responsibility.aspx (accessed January 15, 2018)

[2] Li, C., Fu, L., Stafford, J., Belosevic, M., El-Din, M. G. (2016). The toxicity of oil sands process-affected water (OSPW): A critical review, Sci. Total Environ. 601-602, 1785-1802.

[3] Alberta Energy Regulator, Crude Bitumen Demand, Upgraded and nonupgraded bitumen. http://www.aer.ca/providing-information/data-and-reports/statistical-reports/crude-bitumen-demand (accessed January 15, 2018)

[4] Wiebe-Neufeld, D. A different perspective on Alberta's Oil Patch - Mennonites who work in the industry weigh in on the world's addiction to 'black gold.' http://www.canadianmennonite.org/articles/different-perspective-albertas-oil-patch (accessed January 15, 2018)

[5] Natural Resources Canada. Oil Sands Extraction and Processing. https://www.nrcan.gc.ca/energy/oil-sands/18094 (accessed January 15, 2018)

[6] Butler, R. M. (1994). Steam-Assisted Gravity Drainage: Concept, Development, Performance, and Future, Journal of Canadian Petroleum Technology 33(02), 44-50.

[7] Vedoy, R. L. D, Soares, B. P. J. (2015). Water-Soluble Polymers for Oil Sands Tailing Treatment: A Review, Can. J. Chem. Eng. 93, 888-904

[8] Masliyah, J. H., Czarnecku, J. A., Xu, Z. (2011). Handbook on Theory and Practice of Bitumen Recovery from Athabasca Oil Sands: Theoretical Basis, Volume 1, Kingsley Knowledge, 449

[9] Ramanova, U. G., Valinisab, M., Stasiuk, E. N., Yarraton, H. W., Scharamm, L. L., Shelfantook, W. E. (2006). The Effect of Oil Sands Bitumen Extraction Conditions on Froth Treatment Performance, J. Can. Petrol. Tech. 45, 44

[10] BCG Engineering Inc., 2010, Oil Sands Tailings Technology Review. Oil Sands Research and Information Network, University of Alberta, School of Energy and the Environment, Alberta. ORSIN Report No. TR-1

[11] Mikula, R. J., Kasperski, K. L., R.D. Burns, R. D., MacKinnon, M. D. (1996). Nature and fate of oil sands fine tailings, Advances in Chemistry. 251, 677–723.

[12] Government of Alberta: Environment and Sustainable Resource Department, Environmental Management of Alberta's Oil Sands, 2009.

[13] Chalaturnyk, R. J., Scott, D., Ozum, B. (2002). Management of Oil Sands Tailings, Journal of Petroleum Science and Technology. 20, 1025 – 1046.

[14] Small, C. C., Cho, S., Hashisho, Z., Ulrich, A.C. (2015). Emissions from Oil Sands Tailings Ponds: Review of Tailings Pond Parameters and Emission Estimates, Journal of Petroleum Science and Engineering. 127, 490-501.

[15] Kotlyar, L.S., Sparks, B. D., Woods, J., Capes, C. E., Schutte, R. (1995). Biwetted Ultrafine Solids and Structure Formation in Oil Sands Fine Tailings, Fuel, 74, 1146-1149.

[16] Houlihan, R., Haneed M. (2008). Oil Sands Tailings: Regulatory Perspective. IN: International Oil Sands Tailing Conference, Edmonton, Alberta.

[17] Xu, Y., Dabros, T., Kan, J. (2013). Investigation on alternative disposal methods for froth treatment tailings-part 1, disposal without asphaltene recovery. Canadian Journal of Chemical Engineering, 91(8), 2013, 1349-1357.

[18] Devenny, D.W. (2010). A Screening Study of Oil Sand tailings Technologies and Practices. Prepared for Alberta Energy Research Institute, Edmonton, Alberta. Rev. 1 (2010)

[19] World Wide Fund for Nature (WWF) – Canada (2010). Tailings, A Lasting Oil Sands Legacy.

[20] Shang, J. (1997). Electrokinetic Sedimentation: A Theoretical and Experimental Study, Canadian Geotechnical Journal, 34, 305-314.

[21] Wang, C., Harbottle D., Liu, Q., Xu, Z. (2014). Current State of Fine Mineral Tailings Treatment: A Critical Review of Theory and Practice. Minerals Engineering, 58, 113 – 131.

[22] Proskin, S., Sego, D., Alostaz, M. (2010). Freeze–thaw and Consolidation Tests on Suncor Mature Fine Tailings (MFT), Cold Regions Science and Technology, 63, 110-120.

[23] Li, M., Barbour, S.L., Si, B.C. (2015). Measuring Solid Percentage of Oil Sands Mature Fine Tailings Using the Dual Probe Heat Pulse Method, J. Environ. Qual. 44, 293-298.

[24] Claesson, P.M., Dahlgren, M.A.G., Eriksson, L., (1994). Forces Between Polyelectrolyte Coated Surfaces: Relations Between Surface Interaction and Floc Properties. Colloids Surf. A 93, 293–303.

[25] Alamgir, A., Harbottle, D., Masliyah, J., Xu, Z. (2012). Al-Pam assisted Filtration System for Abatement of Mature Fine Tailings. Chemical Engineering Science, 80, 91-99.

[26] Alberta Energy Regulator, Directive 085: Fluid Tailings Management for Oil Sands Mining Projects (2016).

https://www.aer.ca/documents/directives/Directive085.pdf (accessed January 15, 2018)

[27] Masliyah, J. H., Czarnecki, J., Xu, Z. H. (2011). Handbook on Theory and Practice of Bitumen Recovery from Athabasca Oil Sands. Vol. Volume I: Theoretical Basis. Kingsley Knowledge Publishing.

[28] Hogg, R. (2000). Flocculation and Dewatering, Int. J. Miner. Process. 58, 223-236.

[29] Guo, L. (2012). Understanding Al-PAM assisted oil sands tailings treatment. Diss. University of Alberta.

[30] Oladoja, N. A. (2015). Headway on natural polymeric coagulants in water and wastewater treatment operations, J. Water Process Eng. 6, 174–192.

[31] Ghimici, L., Nichifor, M. (2010). Novel Biodegradable Flocculating Agents Based on Cationic Amphiphilic Polysaccharides, Bioresour. Technol. 101, 8549–8554.

[32] Renault F., Sancey, B., Badot, P.M., Crini, G. (2009). Chitosan for Coagulation/Flocculation Processes – An Eco-Friendly Ppproach, Eur. Polym. J. 45, 1337–1348.

[33] Lee, C. S., Robinson, J., Chong, M. F. (2014). A Review on Application of Flocculants in Wastewater Treatment, Process Safety and Environmental Protection. 92, 489 – 508.

[34] Stocks, P., Parker, K. (2006). "Reagents," Paste and thickened tailings: a guide, 2nd edition, R. J. Jewell, A. B. Fourie, Eds., Australian Centre for Geomechanics, Nedlands, Australia.

[35] Adachi, Y., Kobayashi. A, Kobayahi, M. (2012). Structure of Colloidal Flocs in Relation to the Dynamic Properties of Unstable Suspension. International Journal of Polymer Science. 2012, 14 pgs.

[36] Lu, H., Wang, Y., Li, L., Kotsuchibashi, Y., Narain, R., Zeng, H. (2015). Temperature-and pH-Responsive Benzoboroxole-Based Polymers forFlocculation and Enhanced Dewatering of Fine Particle Suspensions. ACS Appl. Mater. Interfaces, 7 (49), 27176−27187.

[37] Bersa, L., Sengupta, D. K., Roy, S. K. (2000). Particle Characteristics and Their Influence on Dewatering of Kaolin, Calcite and Quartz Suspensions. International Journal of Mineral Processing 59.2, 89 – 112.

[38] Hogg, R., Brunnaul, P., Suharyono, H. (1993). Chemical and Physical Variables in Polymer-Induced Flocculation, Mineral and Metallurg. Processing 10, 81-85.

[39] Sworska, A., Laskowski, J.S., Cymerman, G. (2000). Flocculation of the Syncrude Fine Tailings Part II. Effect of Hydrodynamic Conditions, Int. J. Miner. Process. 60, 153 – 161.

[40] Demoz, A., Mikila, R. J. (2011). Role of Mixing Energy in the Flocculation of Mature Fine Tailings, Journal of Environmental Engineering. 138, 129-136.

[41]Yang, Q.; Song, C.; Chen, Q.; Zhang, P.; Wang, P. Synthesis and Aqueous Solution Properties of Hydrophobically Modified Anionic Acrylamide Copolymers. J. Polym. Sci.

[42] Botha, L., Davey, S., Nguyen, B., Swarnakar, A. K., Rivard, E., Soares, J. B. P. (2017). Flocculation of Oil Sands Tailings by Hyperbranched Functionalized Polyethylenes (HBfPE). Miner. Eng., 108, 71–82. Part B Polym. Phys. 2008, 46 (22), 2465–2474.

[43] Alagha, L., Wang, S., Yan, L., Xu, Z., Masliyah, J. (2013). Probing Adsorption of Polyacrylamide-based Polymers on Anisotropic Basal Planes of Kaolinite Using Quartz Crystal Microbalance. Langmuir, 29 (12), 3989−3998.

[44] Alamgir, A., Harbottle, D., Masliyah, J., Xu, Z. (2012). Al-PAM Assisted Filtration System for Abatement of Mature Fine Tailings. Chem. Eng. Sci., 80, 91−99.

[45] Alagha, L., Wang, S., Xu, Z., Masliyah, J. (2011) Adsorption Kinetics of a Novel Organic−inorganic Hybrid Polymer on Silica and Alumina Studied by Quartz Crystal Microbalance. J. Phys. Chem., 115 (31), 15390−15402.

[46] Li, H., Long, J., Xu, Z., Masliyah, J. (2007). Flocculation of Kaolinite Clay Suspensions Using a Temperature-sensitive Polymer. AIChE J., 53 (2), 479–488.

[47] Wang, Y., Kotsuchinashi, Y., Liu, Y., Narain, R. (2014). Temperature Responsive Hyperbranched Amine-Based Polymers for Solid-Liquid Sepreation, Lagmuir, 2360 – 2368.

[48] O'Shea, J.-P., Qiao, G. G., Franks, G. V. (2012). Temperature-Responsive Solid-Liquid Separations with Charged Block-Copolymers of poly(N-Isopropyl Acryamide). Langmuir, 28 (1), 905–913.

[49] Zhang, D., Thundat, T., Narain, R. (2017). Flocculation and Dewatering of Mature Fine Tailings Using Temperature-Responsive Cationic Polymers. Langmuir, 33 (23), 5900–5909.

[50] Franks, G.V., Sepulveda, C.V., Jameson, G.J., (2006). pH-sensitive Flocculation: Settling Rates and Sediment Densities. AIChEJ. 52, 2774–2782.

[51] Lu, H., Wang, Y., Li, L., Kotsuchibashi, Y., Narain, R., Zeng, H. (2015). Temperature-and pH-Responsive Benzoboroxole-Based Polymers for Flocculation and Enhanced Dewatering of Fine Particle Suspensions. ACS Appl. Mater. Interfaces, 7 (49), 27176−27187.

[52] Wan, C., Alam, M. A., Zhao, X. Q., Zhang, X. Y., Guo, S. L., Ho, S. H., Chang, J. S., Bai, F. W. (2015). Current Progress and Future Prospect of Microalgal Biomass Harvest Using Various Flocculation Technologies. Bioresour. Technol. 2015, 184, 251−257.

[53] Das, R., Ghorai, G. S., Pal, S. (2013). Flocculation Characteristics of Polyacrylamide Grafted Hydroxypropyl Methyl Cellulose: An Eefficient Biodegradable Flocculant. Chem. Eng. J., 229, 144−152.

[54] de Oliveira, L., Gumefekar, S. P., Motta, F. L., Soares, J. B. P. (2018). Dewatering of Oil Sands Tailings with Novel Chitosan-Based Flocculants. Energy Fuels, 32, 5271 – 5278.

[55] Dwivedi, A.D., Dubey, S.P., Hokkanen, S., Sillanpää, M. (2014). Mechanistic Investigation on the Green Recovery of Ionic, Nanocrystalline, and Metallic Gold by Two Anionic Nanocelluloses. Chem. Eng. J. 253, 316–324.

[56] Suopajärvi, T., Liimatainen, H., Hormi, O., Niinimäki, J. (2013) .Coagulation-flocculation Treatment of Municipal Wastewater Based on Anionic Nanocelluloses. Chem. Eng. J. 231, 59–67.

[57] Jin, L., Wei, Y., Xu, Q., Yao, W., Cheng, Z. (2014). Cellulose Nanofibers Prepared from TEMPO-oxidation of Kraft Pulp and its Flocculation Effect of Kaolin Clay. J. Appl. Polym. Sci., 40450 - 40458

[58] Liimatainen, H., Sirviö, J., Sundman, O., Hormi, O., Niinimäki, J. (2012) .Use of Nanoparticular and Soluble Anionic Celluloses in Coagulation-flocculation Treatment of Kaolin Suspension. Water Res. 46, 2159–2166.

[59] Kemppainen, K., Suopajarvi, T., Laitinen, O., Ammala, A., Liimatainen, H., Illikainen, M. (2016). Flocculation of Fine Hematite and Quartz Suspensions with Anionic Cellulose Nanofibers. Chemical Engineering Science, 148, 256 – 266.

[60] Cooley, J.F., inventor. (1902) Apparatus for Electrically Dispersing Fluids, USA patent 692,631.

[61] Taylor, G. (1964). Disintegration of Water Drops in an Electric Field. Proc. Roy. Soc. 280(A), 383-397.

[62] Li D., Xia Y. (2004). Electrospinning of Nanofibers: Reinventing the Wheel, Advanced Materials, 16, No. 14, 1151 – 1170.

[63] Taylor, G. (1969). Electrically Driven Jets. Proceedings of the Royal Society of London. Series A, Mathematical and Physical Sciences, 313, 453 – 475.

[64] Yarin A.L., Koombhongse, S., Reneker, D.H. (2001) Taylor Cone and Jetting from Liquid Droplets in Electrospinning of Nanofibers. Journal of Applied Physics, 90, 4836 – 4846.

[65] Hohman, M. M., Shin, M., Rutledge G. C., Brenner, M. P. (2001). Electrospinning and Electrically Forced Jets. I. Stability Theory, Phys. Fluids 13, 2201 – 2220.

[66]] Hohman, M. M., Shin, M., Rutledge G. C., Brenner, M. P. (2001). Electrospinning and electrically forced jets. II. Applications, Phys. Fluids, 13, 2221 – 2236.

[67] Shin, Y. M., Hohman, M. M., Brenner, M. P., Rutledge G. C. (2001). Electrospinning: A Whipping Fluid Jet Generates Submicron Polymer Fibers, Appl. Phys. Lett. 78, 1149 – 1151.

[68] Renekar, D. H., Yarin, A. L., Fong, H., Koombhongse, S. (2000). Bending Instability of Electrically Charged Liquid Jets of Polymer Solutions in Electrospinning, J. Appl. Phys., 87, 4531 – 4547.

[69] Reneker, D.H. , Yarin, A. L. (2008). Electrospinning Jets and Polymer Nanofibers. Polymer, 49, 2387 – 2425.

[70] Coles, S. R., Jacobd, D. K., Meredith, J. O., Barker, G., Clark, A. J., Kirwam, K., Stranger, J., Tucker, N. (2010). A Design of Experiments (DoE) Approach to Material Properties Optimization of Electrospun Nanofibers. J. Appl. Polym. Sci., 117, 2251 – 2257.

[71] Demir. M. M., Yilgor, I., Yiglor E., Erman, B. (2002). Electrospining of Polyurethan Fibers, Polymer, 43, 3303 – 3309.

[72] Yuan, X., Zhang, Y., Dong C., Sheng, J. (2004). Morphology of Ultrafine Polysulfone Fibers Prepared by Electrospinning, Polym. Int., 53, 1704 – 1710.

[73] Katta, P., Alessandro, M., Ramsier, R.D., Chase, G.G. (2004). Continuous Electrospinning of Aligned Polymer Nanofibers onto A Wire Drum Collector. Nano letters, 4, 2215 – 2218.

[74] Xu, C. Y., Inai, R., Kotaki, M., Ramakrishna, S. (2004). Aligned Biodegradable Nanofibrous Structure: A Potential Scaffold for Blood Vessel Engineering. Biomaterials, 25, 877 – 886.

[75] Seo, J.M., Arumugam, G. K., Khan, S., Heiden, P. A. (2009). Comparison of the Effects of an Ionic Liquid and Triethylbenzylammonium Chloride on the Properties of Electrospun Fibers, 1- Poly(lactic acid). Macromolecular Materials and Engineering, 294, 35 – 44.

[76] Gupta, P., Elkins, C., Long, T. E., Wilkes, G. L. (2005). Electrospinning of Linear Homopolymers of Poly(methyl methacrylate): Exploring Relationships Between Fiber Formation, Viscosity, Molecular Weight and Concentration in a Good Solvent. Polymer, 46, 4799 – 4810.

[77] Koski, A, Yim, K., Shivkumar, S. (2004). Effect of Molecular Weight on Fibrous PVA Produced by Electrospinning. Materials Letter, 58, 493 – 497.

[78] Yang, Q., Li, Z., Hong, Y., Zhao, Y, Qiu, S., Wang, C., Wei, Y. (2004). Influence of Solvents on the Formation of Ultrathin Uniform Poly(vinyl pyrrolidone) Nanofibers with Electrospinning, Poly. Phys., 42, 3721 – 3726.

[79] Eda, G., Liu, J., Shivkumar, S. (2007). Solvent Effects on Jet Evolution During Electrospinning of Semi-dilute Polystyrene Solutions. European Polymer Journal, 43, 1154 – 1167.

[80] Givens, S. R., Gardner, K. H., Rabolt, J. F., Chase D. B. (2007) High-temperature Electrospinning of Polyethylene Microfibers from Solution. Macromolecules, 40, 608 – 610.

[81] Qin, X., Yang, E., Wang. S. (2006). Effect of Different Salts on Electrospinning of Polyacrylonitrile (PAN) Polymer Solution, Journ. App. Poly. Sci., 103, 3865 – 3870.

[82] Casper, L., Stephens, J. S., Nancy G., Tassi, D., Chase, B., Rabolt, J. F. (2003). Controlling Surface Morphology of Electrospun Polystyrene Fibers: Effect of Humidity and Molecular Weight in the Electrospinning Process, Macromolecules, 37, 573 – 578.

[83] Donaldson Company. Ultra-Web Nanofiber Filtration Technology. https://www.donaldson.com/content/dam/donaldson/engine-hydraulics-bulk/literature/north-america/air/F111274-ENG/Ultra-Web-Air-Filtration-Nanofiber-Technology.pdf (accessed January 20, 2018).

[84] Barhate, R.S., Ramakrishna, S. (2007). Nanofibrous Filtering Media: Filtration Problems and Solutions from Tiny Materials. Journal of Membrane Science, 296, 1 – 8.

[85] Li, W., Laurencin, C. T., Caterson, E.J., Tuan, R. S., Ko, F.K. (2002). Electrospun Nanofibrous Structure: A Novel Scaffold for Tissue Engineering, J. Bio. Mater. Res., 60, 613 – 621.

[86] Yoshimoto, H., Shin, Y. M., Terai, H., Vacanti, J.P. (2003). A Biodegradable Nanofiber Scaffold by Electrospinning and its Potential for Bone Tissue Engineering. Biomaterials, 24, 2077 – 2082.

[87] Hu, X., Liu, S., Zhou, G., Huang, Y., Xie, Z., Jing, X. (2014). Electrospinning of Polymeric Nanofibers for Drug Delivery Applications. Journal of Controlled Release, 185, 12 – 21.

[88] Kamble, P., Sadarani, B., Majumdar, A., Bhullar, S. (2017). Nanofiber Based Drug Delivery Dystems for Skin: A Promising Therapeutic Approach. Journal of Drug Delivery Science and Technology, 41, 124 – 133.

[89] Faccini, M., Vaquero, C., Amantia, D. (2012). Development of Protective Clothing against Nanoparticle Based on Electrospun Nanofibers. Journal of Nanomaterials, 1 – 9.

[90] Vitchuli, N., Shi, Q., Nowak, J., McCord, M., Bourham, M., Zhang, X. (2010). Electrospun Ultrathin Nylon Fibers for Protective Applications, Journal of Applied Polymer Science 116, 2181 – 2187.

[91] Gibson, P., Shreuder-Gibson, H., Rivin, D. (2001). Transport properties of Porous Membranes Based on Electrospun Nanofibers. Colloids and Surfaces, 187-188, 469 – 481.

[92] Bedford, N.M., Steckl, A.J. (2010). Photocatalytic Self Cleaning Textile Fibers by Coaxial Electrospinning. Applied Materials and Interfaces, 2, 2448 – 2455.

[93] Liu, Y., Dong, L., Fan, J., Wang, R., Yu, J. (2011). Effect of Applied Voltage on Diameter and Morphology of Ultrafine Fibers in Bubble Electrospinning. Journal of Applied Polymer Science, 120, 592 – 598.

[94] Zhang, X.D., Macosko, C.W., Davis, H.T., Nikolov, A.D., Wasan, D.T. (1999). Role of Silicone Surfactant in Flexible Polyurethane Foam. Journal of Colloidal and Interface Science, 215, 270 – 279.

[95] Hill, R.M. (2002). Silicon Surfactants – New Developments. Current Opinion in Colloidal and Interface Science, 7, 255 – 261.

[96] Hilton, J.E., Van Der Net, A. (2009). Dynamics of Charged Hemispherical Soap Bubbles. EPL, 86 (24003), 1 – 5.

[97] Yang, R., He, J., Yu, J. (2009) Bubble-electrospinning for Fabricating Nanofibers. Polymer, 50, 5846 – 5850.

[98] He, J., Liu, Y. (2012). Control of Bubble Size and Bubble Number in Bubble Electrospinning. Computers and Mathematics with Applications, 64, 1033 – 1035.

[99] Smit, A.E., Sanderson, R.D. (2008). Studies Towards High-Throughput Production of Nanofiber Yarns. University of Stellenbosch.

[100] He, J., Liu, Y., Xu, L., Yu, J., Sun, G. (2008). BioMimic Fabrication of Electrospun Nanofibers with High-Throughput. Chaos Solutions and Fractals, 37, 643 – 651.

[101] Farksih, A., Fall, M. (2013). Rapid Dewatering of Oil Sand Mature Fine Tailings Using Super Absorbent Polymer (SAP). Minerals Engineering, 50 – 51, 38 – 47.

[102] Bourgès-Gastaud, S., Dolez, P., Blond, E., Touze-Foltz, N. (2017). Dewatering of Oil Sands Tailings with an Electrokinetic Geocomposite, Miner. Eng. 100, 177–186

[103] Li, M., Barbour, S.L., Si, B.C. (2015). Measuring Solid Percentage of Oil Sands Mature Fine Tailings Using the Dual Probe Heat Pulse Method, J. Environ. Qual. 44, 293.

[104] Vadodaria, K., Stylios, G.K. (2012). Comparison of Bubble Electrospinning and Needle Electrospinning of Ethylcellulose Ultrafine Fibers. Advanced Materials Research, 622 – 623, 710 – 715.

[105] Zhou, F., Gong, R., Porat, I. (2009). Mass Production of Nanofibre Assemblies bu Electrostatic Spinning. Polym. Int., 58, 331 – 342.

[106] Lu, H., Wang, Y., Li, L., Kotsuchibashi, Y., Narain, R., Zeng, H. (2015). Temperatures- and pH-Responsive Benzobroxole-Based Polymers for Flocculation and Enhanced Dewatering of Fine Particle Suspensions. Appl. Mater. Interfaces, 7, 27176 – 27187.

[107] Olsson, A.L.J., van der Mei, H.C., Johannsmann, D., Busscher, H.J., Sharma, P.K. (2012). Probing Colloid−Substratum Contact Stiffness by Acoustic Sensing in a Liquid Phase. Analytical Chemistry, 84, 4504 – 4512.

[108] Stephens, J.S., Chase, D.B., Rabolt, J.F. (2004). Effect of the Electrospinning Process on Polymer Crystallization Chain Conformation in Nylon-6 and Nylon-12. Macromolecules, 37, 877 – 881.

[109] Nayak, B.R., Singh, R.P. (2001). Synthesis and Characterization of Grafted Hydroxypropyl Guar Gum by Ceric Ion Induced Initiation. European Polymer Journal 37(8), 1655 – 1666

[110] Das, R., Basu, D., Khan, A.K., Banerjee, A. (1998). Graft Copolymerization of Methyl Methacrylate onto Silk Fiber using Ce+3/K2S2O8 as Redox Initiator Under Visible Light in Limited Aqueous Medium. Indian J. Fibre Textile Research 23, 258-288

[111] Lanthong, P., Nuisin., Kiatkamjornwong, S. (2006). Graft Copolymerization, Characterization, and Degradation of Cassava Starch-g-acrylamide/Itaconic Acid Superabsorbents. Carbohydrate Polymers 66(2), 229-245

[112] Lin, Y.Q., Pledger, H.J, Butler, G. (1998). Synthesis and Characterization of Poly(diallyldimethylammonium chloride-g-acrylamide), Journal of Macromolecular Science. Part A, Pure and Applied Chemistry A25(8), 999-1013.

[113] Bi, K. and Zhang, Y. (2012), Kinetic study of the polymerization of dimethyldiallylammonium chloride and acrylamide. J. Appl. Polym. Sci., 125: 1636–1641.

[114] Guan, Q., Zheng, H., Zhai, J., Liu, B., Sun, Y., Wang, Y., Xu, Z. and Zhao, C. (2015). Preparation, characterization, and flocculation performance of P(acrylamide-co-diallyldimethylammonium chloride) by UV-initiated template polymerization. J. Appl. Polym. Sci., 132, 41747,

[115] Zhou, T., Zhang, J., Jingfu, J., Jiang, G., Zhang, J., Qiao, J. (2013). Poly(ethylene glycol) plasticized poly(vinyl alcohol)/ poly(acrylamide-co-diallyldimethylammonium chloride) as alkaline anion-exchange membrane for potential fuel cell applications. Synthetic Metals 167, 43-50.

[116] Bowman, L.M., Cha, C.Y. (2003). Solution properties of poly (N,N-diallyldimethylammonium chloride). Journal of Polymer Science: Polymer Letters Edition, 17(3), 167-173

[117] Vu, C., Canestany, J. (1991). Characterization of cationic water-soluble polyacrylamides.- Journal of Applied Polymer Science, 42 (11), 2857-2869.

[118] Wang, X., Yue, Q., Gao, B., Si, X., Sun, X. and Zhang, S. (2011). Dispersion copolymerization of acrylamide and dimethyl diallyl ammonium chloride in ethanol-water solution. J. Appl. Polym. Sci., 120: 1496–1502.

[119] Gumfekar, S.P., Rooney, T.R., Hutchinson, R.A., Soares, J.B.P. (2017). Dewatering Oil Sands Tailings with Degradable Polymer Flocculants. ACS Appl. Mater. Interfaces, 9 (41), 36290 – 36300.

[120] Olsson, A.L.J., Quevedo, I.R., He, D., Basnet, M., Tufenkji, N. (2013). Using the Quartz Crystal Microbalance with Dissipation Monitoring to Evaluate the Size of Nanoparticles Deposited on Surfaces. ACS Nano., 7, 7833 – 7843.

[121] Chen, Q., Xu, S., Liu, Q., Masliyah, J., Xu, Z. (2016). QCM-D Study of Nanoparticle Interactions. Advances in Colloidal and Interface Science, 233, 93 – 114.

[122] Wang, Y., Kotsuchibashi, Y., Liu, Y., Narain, R. (2015). Study of Bacterial Adhesion on Biomimetic Temperature Responsive Glycopolymer Surfaces. Appl. Mater. Interfaces, 7, 1652 – 1661.

[123] Deer, W.A.; Howie, R.A.; Zussman, J. (1992). An Introduction to the Rock-Forming Minerals (2 ed.). Harlow: Longman.

[124] Niasar, H. S., Li, H., Kasanneni, T. V. R., Ray, M. B., Xu, C. (2016). Surface Amination of Activated Carbon and Petroleum Coke for the Removal of Naphthenic Acids and Treatment of Oil Sands Process Affected Water (OSPW). Chem. Eng. J., 293, 189−199.

[125] Thompson, D. K., Motta, F. L., Soares, J. B. P. (2017). Investigation on the Flocculation of Oil Sands Mature Fine Tailings with Alkoxysilanes. Miner. Eng., 111, 90−99.

[126] Stachewicz, U., Barber, A.H. (2011). Enhanced Wetting Behavior at Electrospun Polyamide Nanofiber Surfaces. Langmuir, 27, 3024 – 3029.

[127] Stachewicz, U., Stone, C.A, Willis, C.R., Barber, A.H. (2012). Charge Assisted Tailoring of Chemical Functionality at Electrospun Nanofiber Surface. Journal of Materials Chemistry, 22, 22935 – 22941.

[128] Su, W.F. (2013). Principles of Polymer Design and Synthesis, Lecture Notes in Chemistry, Springer, 82, 9 – 26.

[129] Gregory, J. (2009). Monitoring Particle Aggregation Processes. Adv. Colloid Interface Sci., 147–148, 109–123.

[130] Senaputra, A., Jones, F., Fawell, P.D., Smith, P.G. (2014). Focused Beam Reflectance Measurement for Monitoring the Extent and Efficiency of Flocculation in Mineral Systems. AIChE J., 60, 251–265.